

# Mars Sample Return ascent trajectory optimisation using Taylor Series integration

Master Thesis

S.D. Petrovic

Faculty Aerospace, Section Spaceflight



# PREFACE

Back in December 2013 Warren Gebbett gave a presentation on his work at the Jet Propulsion Laboratory (JPL) in Pasadena, California, USA and the opportunity for a new student to go and perform research at JPL. At this point I sent in my application together with eight other students. Then at the end of December I heard that I was invited for an interview in the first week of January 2014. In this interview it was concluded that I met all the requirements and that I was the perfect candidate to follow Warren up as the next student at JPL with financial backing of Dutch Space (now Airbus Defence and Space, the Netherlands). Financial backing was also going to be provided by the Stichting Prof.dr.ir. H.J. van der Maas Fonds (Aerospace Engineering Faculty, TU Delft) and the Stichting Universiteitsfonds Delft (TU Delft). Communication with JPL was thus started and in March 2015 it was clear that I would be working for the Mars Program Formulation Office under the supervision of Roby Wilson (Inner Solar System group, NASA JPL). He told me to focus on subjects that dealt with Mars missions. At that point I was doing my internship at DLR Bremen on Lunar rocket ascent and descent, which lasted till June 2015. When I came back to Delft me and my supervisors Erwin Mooij (rockets, trajectories, entry and descent, TU Delft) and Ron Noomen (mission design and orbit analysis, TU Delft) agreed that it would be best to perform a study on these Mars subjects to prepare for my visit to JPL and to formulate proposal thesis topics. The first week at JPL I presented these initial thesis topics to both people from the Inner Solar System group and the Mars program formulation office. The next few weeks were spent choosing and refining one of these topics. This document is the result of the two-month literature study on that topic to prepare for the thesis project.

*S.D. Petrovic  
Pasadena, California, February 2016*

# CONTENTS

<b>Abbreviations</b>	<b>iv</b>
<b>1 Introduction</b>	<b>1</b>
<b>2 Problem background</b>	<b>2</b>
<b>3 Models</b>	<b>3</b>
<b>4 Optimisation</b>	<b>4</b>
<b>5 Standard integration methods</b>	<b>5</b>
<b>6 Taylor series integration</b>	<b>6</b>
6.1 General theory . . . . .	6
6.1.1 Workings of TSI . . . . .	6
6.1.2 Step-size . . . . .	6
6.2 Associated equations . . . . .	6
6.2.1 Auxiliary equations . . . . .	7
6.2.2 Recurrence relations and auxiliary functions. . . . .	10
<b>7 Program optimisation tool</b>	<b>14</b>
7.1 Existing software . . . . .	14
7.1.1 Tudat . . . . .	14
7.1.2 Eigen. . . . .	15
7.1.3 Boost. . . . .	15
7.1.4 PaGMO . . . . .	15
7.1.5 SNOPT . . . . .	16
7.1.6 Mars-GRAM . . . . .	16
7.2 Developed software . . . . .	16
7.2.1 Atmospheric table function fit . . . . .	16
7.2.2 Drag coefficient graph function fit . . . . .	21
7.2.3 RK4 and RKF propagator. . . . .	22
7.2.4 TSI propagator . . . . .	24
7.2.5 Optimiser . . . . .	25
<b>8 Verification and validation</b>	<b>30</b>
8.1 Interpolation . . . . .	30
8.2 RK4 and RKF integrators . . . . .	30
8.3 Taylor Series integration . . . . .	31
8.4 Complete trajectory propagation . . . . .	31
8.5 Optimiser . . . . .	31
8.6 Complete optimisation tool. . . . .	31
<b>9 Results</b>	<b>32</b>
<b>10 Analysis</b>	<b>33</b>
<b>11 Conclusions and recommendations</b>	<b>34</b>
<b>A Mars-GRAM 2005 input file</b>	<b>35</b>
<b>B Atmospheric data fitting</b>	<b>39</b>
B.1 Temperature . . . . .	39
B.2 Density . . . . .	39
<b>Bibliography</b>	<b>48</b>

# ABBREVIATIONS

<b>ACT</b>	Advanced Concepts Team	<b>PaGMO</b>	Parallel Global Multi-objective Optimizer
<b>DE</b>	Differential Evolution	<b>RF</b>	Frame of Reference
<b>ESA</b>	European Space Agency	<b>RKF45</b>	Runge-Kutta-Fehlberg 4 <sup>th</sup> (5 <sup>th</sup> ) order
<b>GLOM</b>	Gross Lift-Off Mass	<b>RKF</b>	Runge-Kutta-Fehlberg
<b>GRAM</b>	Global Reference Atmospheric Model	<b>RK4</b>	Runge-Kutta 4 <sup>th</sup> order
<b>JPL</b>	Jet Propulsion Laboratory	<b>s/c</b>	Spacecraft
<b>MAV</b>	Mars Ascent Vehicle	<b>SNOPT</b>	Sparse Nonlinear Optimizer
<b>MBH</b>	Monotonic Basin Hopping	<b>SQP</b>	Sequential Quadratic Programming
<b>MOLA</b>	Mars Orbiter Laser Altimeter	<b>TSI</b>	Taylor Series integration
<b>MSR</b>	Mars Sample Return	<b>Tudat</b>	TU Delft Astrodynamics Toolbox

# 1

## INTRODUCTION

Mars Sample Return (MSR) has been a mission concept that has been proposed many times in the past two decades. Even today, research into this mission is still being done. And although it is not yet an official project proposal, NASAs Jet Propulsion Laboratory (JPL) is currently working on pre-cursor missions to eventually launch an MSR mission. To prepare for this, research is being conducted on different aspects of MSR, such as the Mars Ascent Vehicle (MAV) responsible for transporting the dirt and soil samples into a Martian orbit and the orbiter which will then transport the samples back to Earth. The current orbiter proposed by JPL is a low-thrust orbiter called Mars 2022. Such an MSR mission requires precise and optimum (optimised for lowest Gross Lift-Off Mass (GLOM)) trajectories to be able to bring back as many samples as possible. But how does one determine the optimum MAV trajectory? Especially when it is combined with the optimum trajectory of the low-thrust orbiter.

The proposed research would focus on the combined optimisation of an MAV trajectory and the trajectory of the low-thrust Mars 2022 orbiter. Also, one hypothesis is that great mass saving can be made if the orbiter and MAV would rendezvous within one single orbital revolution after MAV lift-off. Therefore, the question that should be answered is: what is the optimal trajectory solution for the combined trajectory problem of a high-thrust MAV and a low-thrust Mars orbiter performing a single-revolution rendezvous in Mars orbit? More information on the proposed topic is provided in ??.

A mission such as MSR and the corresponding trajectories can be described in many different reference frames, or Frame of Reference (RF), and the motion of the MAV and the orbiter can be modelled in different ways. Therefore it is important to use the proper equations and environmental models. Also, the trajectory has to be determined or rather a prediction will have to be made. This can be done using integration methods. And finally, the optimum will have to be found using an optimisation method. All these different aspects are addressed in this literature study.

First however, it is important to determine the knowledge that already exists and the research that has already been performed. Therefore, ?? will describe previous sample return missions, low-thrust Spacecraft (s/c) missions, single-revolution rendezvous missions and the research performed in those fields. It will also describe the current MAV designs. Then before mathematically representing the problem it is important to understand in what kind of RF it has to be described. This will be done in ??, followed by the MAV ascent and low-thrust Mars 2022 orbiter model descriptions in ???? respectively. Here, both chapters explain the assumptions and corresponding equations for each phase. One important aspect of the MAV ascent, which sets it apart from other sample return missions, is that Mars has an atmosphere which cannot be neglected. Accordingly ?? describes the different atmospheric models and the trade-off that was performed to decide which model to use in this thesis problem. Then the integration and optimisation are discussed in ?? and chapter 4 respectively. In the integrators chapter, different integration methods are described and a selection is made of the integration methods that will be used. The same is done for the different optimisers. All of this information will be used to define the final thesis topic, which is presented in ??. For some of the aspects that will be treated in the final thesis problem, certain software is already available. A summary of this software is provided in ??. Finally, a proposed schedule is presented in ??, which shows the work which will have to be performed during the thesis work and the time that will have to be spend on each aspect of it. This literature study will serve as a guideline during the thesis project and provide background information for the final thesis report.

# 2

## PROBLEM BACKGROUND

# 3

## MODELS

# 4

## OPTIMISATION



# 5

## STANDARD INTEGRATION METHODS

# 6

## TAYLOR SERIES INTEGRATION

### 6.1. GENERAL THEORY

#### 6.1.1. WORKINGS OF TSI

#### 6.1.2. STEP-SIZE

### 6.2. ASSOCIATED EQUATIONS

In order for TSI to be implemented, the state derivatives have to be modelled as a set of continuous functions which are a function of the state only. The state is described in Equation (6.1), where  $m_{MAV}$  is the mass of the MAV and the subscript  $I$  refers to the inertial frame.

$$\mathbf{r} = \begin{pmatrix} x_I \\ y_I \\ z_I \end{pmatrix} \quad \mathbf{V} = \begin{pmatrix} V_{x_I} \\ V_{y_I} \\ V_{z_I} \end{pmatrix} \quad m_{MAV} \quad (6.1)$$

The corresponding state derivatives are then described by Equation (6.2).

$$\begin{aligned} \dot{x}_I &= V_{x_I} & \ddot{x}_I &= \dot{V}_{x_I} = a_{x_I} \\ \dot{y}_I &= V_{y_I} & \ddot{y}_I &= \dot{V}_{y_I} = a_{y_I} \\ \dot{z}_I &= V_{z_I} & \ddot{z}_I &= \dot{V}_{z_I} = a_{z_I} \end{aligned} \quad \dot{m}_{MAV} = -\frac{T}{g_0 I_{sp}} \quad (6.2)$$

From this point on, the subscript  $I$  is omitted, because the state and the state derivatives are always presented in the inertial frame. The accelerations in the x-, y- and z-direction have three contributing components: gravitational acceleration, drag and thrust. The gravitational acceleration can be directly expressed in the inertial frame however, the drag is presented in the body frame and the thrust is expressed in the propulsion frame. Therefore, both the drag and thrust contributions have to be transformed to the inertial frame using transformation matrices. This then results in the expression for the acceleration vector as shown by Equation (6.3).

$$\begin{pmatrix} a_x \\ a_y \\ a_z \end{pmatrix} = \begin{pmatrix} -\mu_M \frac{x}{r^3} \\ -\mu_M \frac{y}{r^3} \\ -\mu_M \frac{z}{r^3} \end{pmatrix} + \left| \mathbb{T}_z(-\dot{\Omega}_M t_O + \Omega_P) \right|_{\mathbf{R}} \left| \mathbb{T}_z(-\tau) \mathbb{T}_y\left(\frac{\pi}{2} + \delta\right) \right|_{\mathbf{V}} \left| \mathbb{T}_z(-\chi) \mathbb{T}_y(-\gamma) \right|_{\mathbf{B}} \left[ \begin{pmatrix} -\frac{D}{m_{MAV}} \\ 0 \\ 0 \end{pmatrix} + \dots \right. \\ \left. \dots \left| \mathbb{T}_z(-\psi_T) \mathbb{T}_y(-\epsilon_T) \right|_{\mathbf{P}} \begin{pmatrix} \frac{T}{m_{MAV}} \\ 0 \\ 0 \end{pmatrix} \right] \quad (6.3)$$

It can be seen that this set of equations is a function of the current position and many other parameters. These parameters will all have to be written as a function of the current state. This is done in Section 6.2.1

forming auxiliary equations that need to be solved. Then the recurrence relations can be written for the state derivatives and the corresponding auxiliary equations. To avoid lengthy expressions, the set of equations presented in Equation (6.3) and the auxiliary equations are represented using auxiliary functions. Each of the auxiliary functions performs one simple algebraic operation and the collection of these auxiliary functions then form the complete set of recurrence relations using the recurrence relations for the simple algebraic operations. This is all described in Section 6.2.2.

### 6.2.1. AUXILIARY EQUATIONS

For the auxiliary equations, a similar notation will be used as shown by Scott and Martini (2008). Here the equations are denoted by  $x_{number}$  and the corresponding derivatives  $x'_{number}$ . This notation will also be used for the current state and the corresponding state derivatives. This way, Equation (6.1) can be written as Equation (6.4) and the corresponding derivatives can be written as presented by Equation (6.5).

$$\begin{aligned} x_1 &= x & x_4 &= \dot{x} = V_x & x_7 &= m_{MAV} \\ x_2 &= y & x_5 &= \dot{y} = V_y & & \\ x_3 &= z & x_6 &= \dot{z} = V_z & & \end{aligned} \quad (6.4)$$

$$\begin{aligned} x'_1 &= x_4 & x'_4 &= \dot{V}_x = a_x = a_{g,x} + a_{D,x} + a_{T,x} & x'_7 &= \dot{m}_{MAV} = -\frac{T}{g_0 I_{sp}} \\ x'_2 &= x_5 & x'_5 &= \dot{V}_y = a_y = a_{g,y} + a_{D,y} + a_{T,y} & & \\ x'_3 &= x_6 & x'_6 &= \dot{V}_z = a_z = a_{g,z} + a_{D,z} + a_{T,z} & & \end{aligned} \quad (6.5)$$

In this case the thrust and specific impulse are constant, which means that  $x'_7$  is constant and any additional derivative will be zero. Also, neither one of the thrust angles is a function of the state, which means that  $a_T$ , in the body frame, is only a function of  $x_7$  (also see Equation (6.3)). However, both  $a_g$  and  $a_D$  are a function of the position and velocity, where  $a_D$  is also a function of the MAV mass. Furthermore, both the drag and thrust accelerations have to be translated to the inertial frame using five different angles. The transformation from the rotating to the inertial frame is performed using an angle that is a function of time where  $t_O = t_0 + t_{current}$  as shown by Equation (6.3). This leaves 4 angles that are a function of the state.  $a_g$  will be discussed first, followed by the transformation angles and  $a_D$  respectively. For the numbering of all the auxiliary equations goes that the order comes from the manner in which they were all written out on paper. This means that sometimes lower number parameters could contain much higher number parameters without the intermediate parameters defined yet. However, these will all be defined eventually.

### GRAVITATIONAL ACCELERATION

For the gravitational acceleration two auxiliary equations were required since  $r = \sqrt{x^2 + y^2 + z^2}$ . The resulting expressions for the gravitational acceleration are shown in Equation (6.6) with the corresponding auxiliary equations and the derivatives defined in Equation (6.7).

$$\begin{aligned} a_{g,x} &= -\mu_M \frac{x_1}{r^3} = \frac{x_1}{(x_1^2 + x_2^2 + x_3^2)^{3/2}} = -\mu_M \frac{x_1}{x_9} \\ a_{g,y} &= -\mu_M \frac{x_2}{r^3} = \frac{x_2}{(x_1^2 + x_2^2 + x_3^2)^{3/2}} = -\mu_M \frac{x_2}{x_9} \\ a_{g,z} &= -\mu_M \frac{x_3}{r^3} = \frac{x_3}{(x_1^2 + x_2^2 + x_3^2)^{3/2}} = -\mu_M \frac{x_3}{x_9} \end{aligned} \quad (6.6)$$

$$\begin{aligned} x_8 &= x_1^2 + x_2^2 + x_3^2 & x'_8 &= 2x_1x_4 + 2x_2x_5 + 2x_3x_6 \\ x_9 &= x_8^{3/2} & x'_9 &= \frac{3}{2} \frac{x_9x'_8}{x_8} \end{aligned} \quad (6.7)$$

## TRANSFORMATION ANGLES

The angles required for the transformation to go from the body frame to the reference frame are all written as auxiliary functions defined in Equation (6.8). As was mentioned before, the angle represented by  $x_{10}$  is not a function of the state and can therefore be treated as a constant.

$$\begin{aligned}
 x_{10} &= \dot{\Omega}_M t_O - \Omega_P \\
 x_{11} &= \tau = \lambda - x_{10} = \arctan\left(\frac{x_2}{x_1}\right) - x_{10} = \text{atan2}(x_2, x_1) - x_{10} \\
 x_{12} &= \delta = \arcsin\left(\frac{x_3}{r}\right) = \arcsin\left(\frac{x_3}{x_{20}}\right) \\
 x_{13} &= \chi = \arccos\left(\frac{r\dot{\delta}}{V\cos\gamma}\right) = \arccos(x_{22}) \\
 x_{14} &= \gamma = \arcsin\left(\frac{\dot{r}}{V}\right) = \arcsin(x_{23})
 \end{aligned} \tag{6.8}$$

These equations require extra auxiliary equations which are all presented in Equation (6.9).

$$\begin{aligned}
 x_{15} &= V = \sqrt{x_{21}} & x_{22} &= \frac{x_{18}}{x_{17}} \\
 x_{16} &= \cos x_{14} & x_{23} &= \frac{x_{25}}{x_{15}} \\
 x_{17} &= x_{16}x_{15} & x_{24} &= x'_{12} = \dot{\delta} = \frac{x_1 x_5 - x_2 x_4}{x_{19}} \\
 x_{18} &= x_{20}x_{24} & x_{25} &= x'_{20} \\
 x_{19} &= x_1^2 + x_2^2 & x_{26} &= x'_8 \\
 x_{20} &= r = \sqrt{x_8} \\
 x_{21} &= x_4^2 + x_5^2 + x_6^2
 \end{aligned} \tag{6.9}$$

The derivatives of all these auxiliary equations are shown in Equation (6.10).

$$\begin{aligned}
 x'_{10} &= 0 & x'_{18} &= x_{20}x'_{24} + x_{24}x'_{25} \\
 x'_{11} &= \frac{x_{20}x - x_3x_{25}}{x_{20}^2\sqrt{1 - \left(\frac{x_3}{x_{20}}\right)^2}} & x'_{19} &= 2x_1x_4 + 2x_2x_5 \\
 x'_{12} &= \dot{\delta} = \frac{x_1x_5 - x_2x_4}{x_{19}} & x'_{20} &= \frac{x_{26}}{2x_{20}} \\
 x'_{13} &= -\frac{x'_{22}}{\sqrt{1 - x_{22}^2}} & x'_{21} &= 2x_4x'_4 + 2x_5x'_5 + 2x_6x'_6 \\
 x'_{14} &= \frac{x'_{23}}{\sqrt{1 - x_{23}^2}} & x'_{22} &= \frac{x_{17}x'_{18} - x_{18}x'_{17}}{x_{18}^2} \\
 x'_{15} &= \frac{x'_{21}}{2x_{15}} & x'_{23} &= \frac{x_{15}x'_{25} - x_{25}x'_{15}}{x_{25}^2} \\
 x'_{16} &= -\sin x_{14}x'_{14} & x'_{24} &= x''_{12} = \frac{x_{19}(x_5x_4 + x_1x'_5 - x_4x_5 - x_2x'_4) - x'_{19}(x_1x_5 - x_2x_4)}{x_{19}^2} \\
 x'_{17} &= x_{16}x'_{15} + x_{15}x'_{16} & x'_{25} &= x''_{20} = \frac{2x_8x'_{26} - x_{26}^2}{4x_9} \\
 & & x'_{26} &= x''_8 = 2x_{21} + 2(x_1x'_4 + x_2x'_5 + x_3x'_6)
 \end{aligned} \tag{6.10}$$

Please note that in this case  $x'_4$ ,  $x'_5$  and  $x'_6$  of the previous time step are taken.

## DRAG ACCELERATION

The drag acceleration is determined in the body frame by dividing the drag force ( $D$ ) by the mass of the MAV ( $x_7$ ). The drag force itself is a function of the position and velocity. The auxiliary equations associated with the drag function are described in Equation (6.11) and the corresponding derivatives are presented by Equation (6.12) except for the  $C_D$  equations. The polynomial coefficients for the density equation are provided in Table 7.4 and are represented in Equation (6.11) by  $P_\rho$ .

$$\begin{aligned}
x_{27} &= D = \frac{1}{2} \rho V^2 S C_D = \frac{1}{2} S x_{28} x_{15}^2 x_{29} \\
x_{28} &= \rho = e^{x_{30}} \\
x_{29} &= C_D \\
x_{30} &= P_{\rho 10} x_{31}^{10} + P_{\rho 9} x_{31}^9 + P_{\rho 8} x_{31}^8 + P_{\rho 7} x_{31}^7 + P_{\rho 6} x_{31}^6 + P_{\rho 5} x_{31}^5 + P_{\rho 4} x_{31}^4 + P_{\rho 3} x_{31}^3 + P_{\rho 2} x_{31}^2 + P_{\rho 1} x_{31} + P_{\rho 0} \\
x_{31} &= h = r - R_{MOLA} = x_{20} - R_{MOLA}
\end{aligned} \tag{6.11}$$

$$\begin{aligned}
x'_{27} &= \frac{1}{2} S x_{15} (x_{15} (x_{29} x'_{28} + x_{28} x'_{29}) + 2 x_{28} x_{29} x'_{15}) \\
x'_{28} &= x'_{30} e^{x_{30}} \\
x'_{30} &= x'_{31} (10 P_{\rho 10} x_{31}^9 + 9 P_{\rho 9} x_{31}^8 + 8 P_{\rho 8} x_{31}^7 + 7 P_{\rho 7} x_{31}^6 + 6 P_{\rho 6} x_{31}^5 + 5 P_{\rho 5} x_{31}^4 + 4 P_{\rho 4} x_{31}^3 + 3 P_{\rho 3} x_{31}^2 + 2 P_{\rho 2} x_{31} + P_{\rho 1}) \\
x'_{31} &= x'_{20}
\end{aligned} \tag{6.12}$$

Since the drag coefficient is a function of Mach number as by Figure 7.10 and is not a continuous function, it had to be split into 6 different sections. Each section has a separate  $C_D - M$  relation. Before these relations can be described, three additional auxiliary equations/expressions are required which are described in Equation (6.13).

$$\begin{aligned}
x_{32} &= M = \frac{V}{a} = \frac{x_{15}}{x_{33}} \\
x_{33} &= a = \sqrt{\gamma_a R_a^* T_a} = \sqrt{\gamma_a R_a^* x_{34}} \quad \text{where} \quad R_a^* = \frac{R_a}{M_a} \\
x_{34} &= T_a
\end{aligned} \tag{6.13}$$

The conditional relations shown in Equation (6.14) describe the different auxiliary equations that have to be used associated with the different sections. Here  $P_{C_D \text{ number, section}}$  are the polynomial fit coefficients as provided in Table 7.5.

$$x_{29} = C_D = \begin{cases} x_{29,1} = 0.2, & \text{for } 0 \leq x_{32} < 0.5 \\ x_{29,2} = P_{C_D 1,2} x_{32} + P_{C_D 0,2}, & \text{for } 0.5 \leq x_{32} < 1 \\ x_{29,3} = P_{C_D 1,3} x_{32} + P_{C_D 0,3}, & \text{for } 1 \leq x_{32} < 1.3 \\ x_{29,4} = P_{C_D 1,4} x_{32} + P_{C_D 0,4}, & \text{for } 1.3 \leq x_{32} < 2.5 \\ x_{29,5} = P_{C_D 1,5} x_{32} + P_{C_D 0,5}, & \text{for } 2.5 \leq x_{32} < 4 \\ x_{29,6} = 0.3, & \text{for } x_{32} \geq 4 \end{cases} \tag{6.14}$$

The corresponding derivatives are presented Equation (6.15).

$$x'_{29} = \begin{cases} x'_{29,1} = 0, & \text{for } 0 \leq x_{32} < 0.5 \\ x'_{29,2} = P_{C_D 1,2} x'_{32}, & \text{for } 0.5 \leq x_{32} < 1 \\ x'_{29,3} = P_{C_D 1,3} x'_{32}, & \text{for } 1 \leq x_{32} < 1.3 \\ x'_{29,4} = P_{C_D 1,4} x'_{32}, & \text{for } 1.3 \leq x_{32} < 2.5 \\ x'_{29,5} = P_{C_D 1,5} x'_{32}, & \text{for } 2.5 \leq x_{32} < 4 \\ x'_{29,6} = 0, & \text{for } x_{32} \geq 4 \end{cases} \tag{6.15}$$

The Mach derivative and corresponding speed of sound derivative are described in Equation (6.16).

$$\begin{aligned}
x'_{32} &= \frac{x_{33} x'_{15} - x_{15} x'_{33}}{x_{33}^2} \\
x'_{33} &= \frac{\gamma_a R_a^*}{2 x_{33}} x'_{34}
\end{aligned} \tag{6.16}$$

This only leaves the temperature  $T_a$ , which is a function of the altitude  $h$  ( $x_{31}$ ) in km, Mars Orbiter Laser Altimeter (MOLA). But as described in Section 7.2.1, this parameter is split into different sections as well. The auxiliary equations per section for the temperature is provided in Equation (6.17). Here  $P_{Tnumber,section}$  are the polynomial fit coefficients as provided in Table 7.2.

$$x_{34} = T = \begin{cases} x_{34,1} = P_{T1,1}x_{31} + P_{T0,1}, & \text{for } -0.6 \leq x_{31} < 5.04 \\ x_{34,2} = P_{T3,2}x_{31}^3 + P_{T2,2}x_{31}^2 + P_{T1,2}x_{31} + P_{T0,2}, & \text{for } 5.04 \leq x_{31} < 35.53 \\ x_{34,3} = P_{T6,3}x_{31}^6 + P_{T5,3}x_{31}^5 + P_{T4,3}x_{31}^4 + P_{T3,3}x_{31}^3 + P_{T2,3}x_{31}^2 + P_{T1,3}x_{31} + P_{T0,3}, & \text{for } 35.53 \leq x_{31} < 75.07 \\ x_{34,4} = P_{T8,4}x_{31}^8 + P_{T7,4}x_{31}^7 + \dots + P_{T3,4}x_{31}^3 + P_{T2,4}x_{31}^2 + P_{T1,4}x_{31} + P_{T0,4}, & \text{for } 75.07 \leq x_{31} < 170.05 \\ x_{34,5} = 136.5, & \text{for } x_{31} \geq 170.05 \end{cases} \quad (6.17)$$

The corresponding derivatives are presented Equation (6.18).

$$x'_{34} = \begin{cases} x'_{34,1} = P_{T1,1}x'_{31}, & \text{for } -0.6 \leq x_{31} < 5.04 \\ x'_{34,2} = (3P_{T3,2}x_{31}^2 + 2P_{T2,2}x_{31} + P_{T1,2})x'_{31}, & \text{for } 5.04 \leq x_{31} < 35.53 \\ x'_{34,3} = (6P_{T6,3}x_{31}^5 + 5P_{T5,3}x_{31}^4 + 4P_{T4,3}x_{31}^3 + 3P_{T3,3}x_{31}^2 + P_{T2,3}x_{31} + P_{T1,3})x'_{31}, & \text{for } 35.53 \leq x_{31} < 75.07 \\ x'_{34,4} = (8P_{T8,4}x_{31}^7 + 7P_{T7,4}x_{31}^6 + \dots + 3P_{T3,4}x_{31}^2 + 2P_{T2,4}x_{31} + P_{T1,4})x'_{31}, & \text{for } 75.07 \leq x_{31} < 170.05 \\ x'_{34,5} = 0, & \text{for } x_{31} \geq 170.05 \end{cases} \quad (6.18)$$

For both the conditional parameters  $C_D$  ( $x_{29}$ ) and  $T_a$  ( $x_{34}$ ) the required section has to be determined before the evaluation of the auxiliary equations.

### 6.2.2. RECURRENCE RELATIONS AND AUXILIARY FUNCTIONS

To be able to determine the different auxiliary functions and eventually write the recurrence relations each of the derivatives presented in Section 6.2.1 will be rewritten using Equation (6.19) as by Scott and Martini (2008).

$$u_n = x'_n, \quad n = 1, \dots, 34 \quad (6.19)$$

These equations are then written as presented by Equations (6.20) and (6.21).

$$\begin{aligned} u_1 &= x_4 \\ u_2 &= x_5 \\ u_3 &= x_6 \\ u_4 &= \dot{V}_x = a_x = a_{g,x} + a_{D,x} + a_{T,x} \\ u_5 &= \dot{V}_y = a_y = a_{g,y} + a_{D,y} + a_{T,y} \\ u_6 &= \dot{V}_z = a_z = a_{g,z} + a_{D,z} + a_{T,z} \\ u_7 &= \dot{m}_{MAV} = -\frac{T}{g_0 I_{sp}} \\ u_8 &= 2x_1x_4 + 2x_2x_5 + 2x_3x_6 \\ u_9 &= \frac{3}{2} \frac{x_9x'_8}{x_8} \\ u_{10} &= 0 \\ u_{11} &= \frac{x_{20}x - x_3x_{25}}{x_{20}^2 \sqrt{1 - \left(\frac{x_3}{x_{20}}\right)^2}} \\ u_{12} &= \dot{\delta} = \frac{x_1x_5 - x_2x_4}{x_{19}} \\ u_{13} &= -\frac{u_{22}}{\sqrt{1 - x_{22}^2}} \\ u_{14} &= \frac{u_{23}}{\sqrt{1 - x_{23}^2}} \\ u_{15} &= \frac{u_{21}}{2x_{15}} \\ u_{16} &= -\sin x_{14} u_{14} \\ u_{17} &= x_{16}u_{15} + x_{15}u_{16} \\ u_{18} &= x_{20}u_{24} + x_{24}x_{25} \\ u_{19} &= 2x_1x_4 + 2x_2x_5 \\ u_{20} &= \frac{x_{26}}{2x_{20}} \end{aligned} \quad (6.20)$$

$$\begin{aligned}
u_{21} &= 2x_4 u_4 + 2x_5 u_5 + 2x_6 u_6 \\
u_{22} &= \frac{x_{17} u_{18} - x_{18} u_{17}}{x_{18}^2} \\
u_{23} &= \frac{x_{15} u_{25} - x_{25} u_{15}}{x_{25}^2} \\
u_{24} &= \frac{x_{19} (x_5 x_4 + x_1 u_5 - x_4 x_5 - x_2 u_4) - u_{19} (x_1 x_5 - x_2 x_4)}{x_{19}^2} \\
u_{25} &= \frac{2x_8 u_{26} - x_{26}^2}{4x_9} \\
u_{26} &= 2x_{21} + 2(x_1 u_4 + x_2 u_5 + x_3 u_6) \\
u_{27} &= \frac{1}{2} S x_{15} (x_{15} (x_{29} u_{28} + x_{28} u_{29}) + 2x_{28} x_{29} u_{15}) \\
u_{28} &= u_{30} e^{x_{30}} \\
u_{29} &= \begin{cases} u_{29,1} = 0, & \text{for } 0 \leq x_{32} < 0.5 \\ u_{29,2} = P_{CD,1,2} u_{32}, & \text{for } 0.5 \leq x_{32} < 1 \\ u_{29,3} = P_{CD,1,3} u_{32}, & \text{for } 1 \leq x_{32} < 1.3 \\ u_{29,4} = P_{CD,1,4} u_{32}, & \text{for } 1.3 \leq x_{32} < 2.5 \\ u_{29,5} = P_{CD,1,5} u_{32}, & \text{for } 2.5 \leq x_{32} < 4 \\ u_{29,6} = 0, & \text{for } x_{32} \geq 4 \end{cases} \\
u_{30} &= u_{31} (10P_{\rho 10} x_{31}^9 + 9P_{\rho 9} x_{31}^8 + 8P_{\rho 8} x_{31}^7 + 7P_{\rho 7} x_{31}^6 + 6P_{\rho 6} x_{31}^5 + 5P_{\rho 5} x_{31}^4 + 4P_{\rho 4} x_{31}^3 + 3P_{\rho 3} x_{31}^2 + 2P_{\rho 2} x_{31} + P_{\rho 1}) \\
u_{31} &= u_{20} \\
u_{32} &= \frac{x_{33} u_{15} - x_{15} u_{33}}{x_{33}^2} \\
u_{33} &= \frac{\gamma_a R_a^*}{2x_{33}} u_{34} \\
u_{34} &= \begin{cases} u_{34,1} = P_{T1,1} u_{31}, & \text{for } -0.6 \leq x_{31} < 5.04 \\ u_{34,2} = (3P_{T3,2} x_{31}^2 + 2P_{T2,2} x_{31} + P_{T1,2}) u_{31}, & \text{for } 5.04 \leq x_{31} < 35.53 \\ u_{34,3} = (6P_{T6,3} x_{31}^5 + 5P_{T5,3} x_{31}^4 + 4P_{T4,3} x_{31}^3 + 3P_{T3,3} x_{31}^2 + P_{T2,3} x_{31} + P_{T1,3}) u_{31}, & \text{for } 35.53 \leq x_{31} < 75.07 \\ u_{34,4} = (8P_{T8,4} x_{31}^7 + 7P_{T7,4} x_{31}^6 + \dots + 3P_{T3,4} x_{31}^2 + 2P_{T2,4} x_{31} + P_{T1,4}) u_{31}, & \text{for } 75.07 \leq x_{31} < 170.05 \\ u_{34,5} = 0, & \text{for } x_{31} \geq 170.05 \end{cases} \quad (6.21)
\end{aligned}$$

As can be seen in Equation (6.20)  $u_4$ ,  $u_5$  and  $u_6$  still have to be written out to include all the accelerations and the transformations. The gravitational accelerations were already written out in Equation (6.6). Then using the convention established in Section 6.2.1 the equation described in Equation (6.3) can be rewritten to the form presented in Equation (6.22) where the transformation matrices are described by Equations (6.23) and (6.24) for  $\mathbb{T}_{\mathbf{BP}}$  and  $\mathbb{T}_{\mathbf{IB}}$  respectively.

$$\begin{pmatrix} u_4 \\ u_5 \\ u_6 \end{pmatrix} = \begin{pmatrix} -\mu_M \frac{x_1}{x_9} \\ -\mu_M \frac{x_2}{x_9} \\ -\mu_M \frac{x_3}{x_9} \end{pmatrix} + \mathbb{T}_{\mathbf{IB}} \left[ \begin{pmatrix} -\frac{x_{27}}{0} \\ \frac{x_7}{0} \\ 0 \end{pmatrix} + \mathbb{T}_{\mathbf{BP}} \begin{pmatrix} \frac{T}{x_7} \\ 0 \\ 0 \end{pmatrix} \right] \quad (6.22)$$

$$\mathbb{T}_{\mathbf{BP}} = \begin{bmatrix} c\psi_T c\epsilon_T & -s\psi_T & c\psi_T s\epsilon_T \\ s\psi_T c\epsilon_T & c\psi_T & s\psi_T s\epsilon_T \\ -s\epsilon_T & 0 & c\epsilon_T \end{bmatrix} \quad (6.23)$$

$$\begin{aligned}
\mathbb{T}_{\mathbf{IB}} &= \begin{bmatrix} c(\dot{\Omega}_M t_O - \Omega_P + \tau)(-s\delta c\chi c\gamma + c\delta s\gamma) - s(\dot{\Omega}_M t_O - \Omega_P + \tau)s\chi c\gamma & c(\dot{\Omega}_M t_O - \Omega_P + \tau)s\delta s\chi - s(\dot{\Omega}_M t_O - \Omega_P + \tau)c\chi \\ s(\dot{\Omega}_M t_O - \Omega_P + \tau)(-s\delta c\chi c\gamma + c\delta s\gamma) + c(\dot{\Omega}_M t_O - \Omega_P + \tau)s\chi c\gamma & s(\dot{\Omega}_M t_O - \Omega_P + \tau)s\delta s\chi + c(\dot{\Omega}_M t_O - \Omega_P + \tau)c\chi \\ c\delta c\chi c\gamma - c\delta s\gamma & -c\delta s\chi \end{bmatrix} \\
&\quad \begin{bmatrix} c(\dot{\Omega}_M t_O - \Omega_P + \tau)(-s\delta c\chi s\gamma - c\delta c\gamma) - s(\dot{\Omega}_M t_O - \Omega_P + \tau)s\chi s\gamma \\ s(\dot{\Omega}_M t_O - \Omega_P + \tau)(-s\delta c\chi s\gamma - c\delta c\gamma) + c(\dot{\Omega}_M t_O - \Omega_P + \tau)s\chi s\gamma \\ c\delta c\chi s\gamma - s\delta c\gamma \end{bmatrix} \\
&= \begin{bmatrix} c(x_{10} + x_{11})(-sx_{12}cx_{13}c\gamma + cx_{12}sx_{14}) - s(x_{10} + x_{11})sx_{13}cx_{14} & c(x_{10} + x_{11})sx_{12}sx_{13} - s(x_{10} + x_{11})cx_{13} \\ s(x_{10} + x_{11})(-sx_{12}cx_{13}cx_{14} + cx_{12}sx_{14}) + c(x_{10} + x_{11})sx_{13}cx_{14} & s(x_{10} + x_{11})sx_{12}sx_{13} + c(x_{10} + x_{11})cx_{13} \\ cx_{12}cx_{13}cx_{14} - cx_{12}sx_{14} & -cx_{12}sx_{13} \end{bmatrix} \\
&\quad \begin{bmatrix} c(x_{10} + x_{11})(-sx_{12}cx_{13}sx_{14} - cx_{12}cx_{14}) - s(x_{10} + x_{11})sx_{13}sx_{14} \\ s(x_{10} + x_{11})(-sx_{12}cx_{13}sx_{14} - cx_{12}cx_{14}) + c(x_{10} + x_{11})sx_{13}sx_{14} \\ cx_{12}cx_{13}sx_{14} - sx_{12}cx_{14} \end{bmatrix}
\end{aligned} \tag{6.24}$$

Because the thrust is constant and the mass flow rate is constant as well, the first derivative of  $u_7$  will be zero such that  $u_7' = 0$ . This means that only the first derivative of the mass flow rate has to be used. Furthermore, the thrust related equations are all treated as constant as well such that the last part of Equation (6.22) can be rewritten to Equation (6.25) using Equation (6.23).

$$\mathbb{T}_{\mathbf{BP}} \begin{pmatrix} \frac{T}{x_7} \\ x_7 \\ 0 \\ 0 \end{pmatrix} = \begin{pmatrix} \frac{T}{x_7} c\psi_T c\epsilon_T \\ \frac{x_7}{T} s\psi_T c\epsilon_T \\ \frac{T}{x_7} s\epsilon_T \end{pmatrix} = \begin{pmatrix} a_{T_B,x} \\ a_{T_B,y} \\ a_{T_B,z} \end{pmatrix} \tag{6.25}$$

The thrust accelerations are now written in the body frame, which means that they can be combined with the drag acceleration in the body frame. This is done in Equation (6.26). However, since the drag acceleration includes an auxiliary equation (for the drag) the total acceleration in the body frame in the x-direction has to be expressed as an auxiliary function. Each auxiliary function replaces one algebraic operation such as multiplication, division, power, exponential and trigonometric functions. Auxiliary functions will be represented by  $w_n$  as per convention introduced by Scott and Martini (2008). These auxiliary functions will be used to write the different parameters into recurrence relations.

$$\begin{pmatrix} -\frac{x_{27}}{x_7} \\ x_7 \\ 0 \\ 0 \end{pmatrix} + \begin{pmatrix} a_{T_B,x} \\ a_{T_B,y} \\ a_{T_B,z} \end{pmatrix} = \begin{pmatrix} a_{T_B,x} - \frac{x_{27}}{x_7} \\ a_{T_B,y} \\ a_{T_B,z} \end{pmatrix} = \begin{pmatrix} a_{T,D_B,x} \\ a_{T_B,y} \\ a_{T_B,z} \end{pmatrix} = \begin{pmatrix} w_1 \\ a_{T_B,y} \\ a_{T_B,z} \end{pmatrix} \tag{6.26}$$

Now transforming the drag and thrust accelerations from the body frame to the inertial frame using  $\mathbb{T}_{\mathbf{IB}}$  results in Equation (6.27).

$$\begin{aligned}
\begin{pmatrix} a_{T,D_I,x} \\ a_{T_I,y} \\ a_{T_I,z} \end{pmatrix} &= \mathbb{T}_{\mathbf{IB}} \begin{pmatrix} a_{T,D_B,x} \\ a_{T_B,y} \\ a_{T_B,z} \end{pmatrix} = \mathbb{T}_{\mathbf{IB}} \begin{pmatrix} w_1 \\ a_{T_B,y} \\ a_{T_B,z} \end{pmatrix} \\
&= \begin{pmatrix} w_1(c(x_{10} + x_{11})(-sx_{12}cx_{13}c\gamma + cx_{12}sx_{14}) - s(x_{10} + x_{11})sx_{13}cx_{14}) + a_{T_B,y}(c(x_{10} + x_{11})sx_{12}sx_{13} - s(x_{10} + x_{11})cx_{13}) + \dots \\ w_1(s(x_{10} + x_{11})(-sx_{12}cx_{13}cx_{14} + cx_{12}sx_{14}) + c(x_{10} + x_{11})sx_{13}cx_{14}) + a_{T_B,y}(s(x_{10} + x_{11})sx_{12}sx_{13} + c(x_{10} + x_{11})cx_{13}) + \dots \\ w_1(cx_{12}cx_{13}cx_{14} - cx_{12}sx_{14}) - a_{T_B,y}cx_{12}sx_{13} + \dots \\ \dots + a_{T_B,z}(c(x_{10} + x_{11})(-sx_{12}cx_{13}sx_{14} - cx_{12}cx_{14}) - s(x_{10} + x_{11})sx_{13}sx_{14}) \\ \dots + a_{T_B,z}(s(x_{10} + x_{11})(-sx_{12}cx_{13}sx_{14} - cx_{12}cx_{14}) + c(x_{10} + x_{11})sx_{13}sx_{14}) \\ \dots + a_{T_B,z}(cx_{12}cx_{13}sx_{14} - sx_{12}cx_{14}) \end{pmatrix}
\end{aligned} \tag{6.27}$$

Now including the gravity components as well, the (lengthy) expressions for  $u_4$ ,  $u_5$  and  $u_6$  become Equations (6.28) to (6.30) respectively.



$$\begin{aligned}
u_4 = & -\mu_M \frac{x_1}{x_9} + w_1 (c(x_{10} + x_{11}) (-sx_{12}cx_{13}c\gamma + cx_{12}sx_{14}) - s(x_{10} + x_{11}) sx_{13}cx_{14}) \\
& + a_{T_B,y} (c(x_{10} + x_{11}) sx_{12}sx_{13} - s(x_{10} + x_{11}) cx_{13}) \\
& + a_{T_B,z} (c(x_{10} + x_{11}) (-sx_{12}cx_{13}sx_{14} - cx_{12}cx_{14}) - s(x_{10} + x_{11}) sx_{13}sx_{14})
\end{aligned} \tag{6.28}$$

$$\begin{aligned}
u_5 = & -\mu_M \frac{x_2}{x_9} + w_1 (s(x_{10} + x_{11}) (-sx_{12}cx_{13}cx_{14} + cx_{12}sx_{14}) + c(x_{10} + x_{11}) sx_{13}cx_{14}) \\
& + a_{T_B,y} (s(x_{10} + x_{11}) sx_{12}sx_{13} + c(x_{10} + x_{11}) cx_{13}) \\
& + a_{T_B,z} (s(x_{10} + x_{11}) (-sx_{12}cx_{13}sx_{14} - cx_{12}cx_{14}) + c(x_{10} + x_{11}) sx_{13}sx_{14})
\end{aligned} \tag{6.29}$$

$$u_6 = -\mu_M \frac{x_3}{x_9} + w_1 (cx_{12}cx_{13}cx_{14} - cx_{12}sx_{14}) - a_{T_B,y} cx_{12}sx_{13} + a_{T_B,z} (cx_{12}cx_{13}sx_{14} - sx_{12}cx_{14}) \tag{6.30}$$

Both  $u_4$  and  $u_5$  are a function of  $x_{11}$  (or the longitude), which includes the atan2 function. It is however more useful to write the longitude as a function of either a sine or cosine. This could be achieved using Figure 6.1, resulting in Equation (6.31).

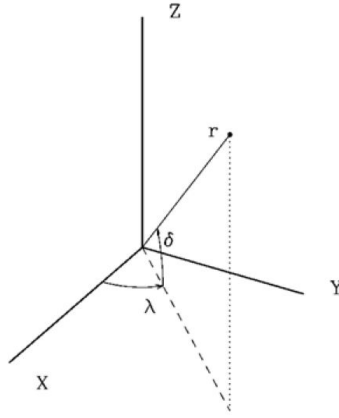


Figure 6.1: Relation between spherical position coordinates and Cartesian position coordinates Noomen (2013)

$$x_{11} = \tau = \lambda - x_{10} = \text{acos2}(x_2, x_1) - x_{10} \tag{6.31}$$

Here the *acos2* function is presented by Equation (6.32). Please note that *acos2* is a function as named by the author of this thesis.

$$\text{acos2}(y, x) = \begin{cases} \frac{y}{|y|} \arccos\left(\frac{x}{\sqrt{x^2 + y^2}}\right), & \text{for } y \neq 0 \\ \arccos\left(\frac{x}{\sqrt{x^2 + y^2}}\right), & \text{for } y = 0, x \neq 0 \\ \text{Undefined}, & \text{for } y = 0, x = 0 \end{cases} \tag{6.32}$$

The new expressions for the longitude now provide the same solutions as the *atan2* function.

# 7

## PROGRAM OPTIMISATION TOOL

To perform the analysis associated with this thesis, a simulation and optimisation program is used. This optimisation tool is comprised of both existing (Section 7.1) and newly developed software (Section 7.2). It is written in C++ and is based on the [Tudat](#) structure. The purpose of the software is to simulate the trajectory of the [MAV](#) and optimise this trajectory with respect to the lowest propellant mass required. This tool is written such that the performance of Runge-Kutta-Fehlberg 4<sup>th</sup> (5<sup>th</sup>) order ([RK45](#)) and [TSI](#) can be compared.

### 7.1. EXISTING SOFTWARE

The use of existing software can greatly improve the performance of the final tool and save time as well. Another important reason to use existing software is that this will make it easier for other people to use and incorporate into their software as well. The existing software used for this thesis is software that is currently being used by the space department of the TU Delft and (in case of [SNOPT](#) and Mars-[GRAM](#)) by the mission design section at [JPL](#).

#### 7.1.1. TUDAT

[Tudat](#) is, as the name suggests, a toolbox that can be used to solve numerous astrodynamic problems ([Dirkx et al., 2016](#)). It was and still is being developed by students and staff of the Delft University of Technology. Specifically by the section Astrodynamics and Space missions of the Aerospace Engineering faculty. It is programmed in C++ and consists of a number of libraries. These libraries can be called upon by the user to invoke different [Tudat](#) functionalities such as standard reference frame transformations or often used integrators. The available software is completely validated and comes with its own tests to make sure that everything is working properly. It itself uses two external libraries: Eigen and Boost. Both these libraries will be discussed in Sections 7.1.2 and 7.1.3 respectively. Figure 7.1 shows [Tudat](#) with the different libraries that are used within the [Tudat](#) Bundle including the core functions ([Tudat Core](#)). In this thesis, the [Tudat](#) libraries are used for all standard mathematical and astrodynamic operations.



Figure 7.1: [Tudat](#) structure

### 7.1.2. EIGEN

Eigen is an external C++ library that was written to perform linear algebra computations<sup>1</sup>. The software is free and easy to use, which is why it is widely used by the C++ community and thus also within *Tudat* (Dirkx et al., 2016). Another advantage is that because it does not use any source files, it does not need to be build before using it. The Eigen libraries contain a number of standardized matrices and vectors, each with its own characteristics. An example of an often used vector is *Vector3d* (or *Eigen::Vector3d*), which can for instance be used to store the Cartesian position of a satellite. Here the 3 shows that it can store 3 values/parameters and the *d* shows that these are of the type *double*. It is mentioned on the *Tudat* wiki (Dirkx et al., 2016) that these Eigen vectors and matrices should only be used if required for linear algebra computations. For ordinary storage, the C++ arrays, vectors and matrices should be used to save both storage and computation time.

### 7.1.3. BOOST

Boost is a slightly more complicated set of C++ libraries, where compared to the Eigen library, Boost first has to be compiled before being able to use all of its functionalities. Fortunately, this compiling is performed by *Tudat* automatically when setting it up for the first time. Boost is described as an addition to the standard C++ libraries, thus adding more functionalities (Dirkx et al., 2016)<sup>2</sup>. Within *Tudat*, Boost is used to pass free and class functions as an argument to another object and also for dynamic allocation using so-called pointers. Four libraries that are often used within *Tudat* are *boost::function*, *boost::bind*, *boost::shared\_ptr* and *boost::make\_shared*. The first two libraries are used to pass functions (a function is pointed to by *function* and called by *bind*) and the last two are used in case of dynamic allocation (*shared\_ptr* is the pointer and *make\_shared* is the object creator that returns a shared pointer to the created object).

### 7.1.4. PAGMO

*PaGMO* is a free optimisation tool developed by European Space Agency (ESA)s Advanced Concepts Team (ACT). It uses parallel computations to perform the optimisation and can even optimise for multi-objective problems. Parallel computation is the act of performing multiple computations on the same machine using different CPU cores. This allows the cost function to be computed for different sets of optimisation parameters at the same time and thus reducing the total CPU time required. However, this only works if the cost function evaluations are independent, which is not always the case (e.g. Dynamic Differential Evolution (DE) described by Qing (2009)). The tool itself incorporates many different local and global optimisation methods as mentioned by Izzo (2012), among which the optimisation method used in this thesis Monotonic Basin Hopping (MBH). This method has been written in *PaGMO* in such a way that it can use any of the provided local optimisers. *PaGMO* is written in C++ and requires the shared libraries of Boost to run<sup>3</sup>. Interfaces to external libraries are also provided, which can incorporate for instance *SNOPT* as a local optimisation method. In this thesis *SNOPT* is used as the local optimiser for MBH as implemented by *PaGMO*. More information on *SNOPT* is provided in Section 7.1.5. For *SNOPT* to be recognised by *PaGMO*, it has to be installed separately. Figure 7.2 shows *PaGMO* with the internally used Boost library and the externally called *SNOPT* software.

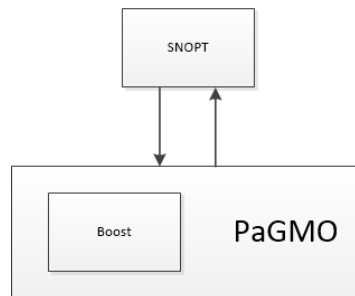


Figure 7.2: *PaGMO* structure

<sup>1</sup>More documentation on Eigen can be found on [eigen.tuxfamily.org/dox/](http://eigen.tuxfamily.org/dox/) [Accessed 8 March 2016]

<sup>2</sup>More documentation on Boost can be found on <http://www.boost.org/> [Accessed 8 March 2016]

<sup>3</sup>More documentation on *PaGMO* can be found on <https://esa.github.io/pagmo/> [Accessed 9 March 2016]

### 7.1.5. SNOPT

**SNOPT** was introduced by Gill *et al.* (2002) as a Sequential Quadratic Programming (**SQP**) method. It uses the first function derivatives and is very effective with highly constrained problems such as trajectory optimisation. Because it is based on **SQP** it is only able to find the local optimum and it is thus not guaranteed that this is also the global optimum. By combining **SNOPT** and **MBH** the global optimum can indeed be found or approached. The tool itself does not require that many evaluations, which is why it is very useful for complex problems with many optimisation variables (Gill *et al.*, 2008). The code for **SNOPT** has been written in Fortran, but can easily be translated to C,C++ using *f2c* which is provided with **SNOPT** as well <sup>4</sup>. This way it can be called by **PaGMO**. It should be noted that **SNOPT** is not free and can only be used under a licence agreement.

### 7.1.6. MARS-GRAM

**Mars-GRAM** is a high-fidelity atmospheric model developed by NASA to simulate the global atmospheric conditions on Mars (Justh and Justus, 2008) <sup>5</sup>. The model is based on NASA Ames Mars General Circulation Model (for altitudes between 0-80 km) and Mars Thermospheric General Circulation model (for altitude above 80 km). It can provide density, temperature and pressure data (among other data) with respect to the current altitude, latitude and longitude on Mars. Seasonal variations are taken into account in the model as well, which is why different calendar dates will result in different atmospheric compositions. The tool can be used within a simulation tool or as a separate executable. Unfortunately, because it is so detailed, each computation requires a lot of CPU time. This is why it was decided to use the stand-alone **Mars-GRAM** executable to generate a detailed table with atmospheric data as a function of altitude, latitude and longitude at the start of the optimisation. Even generating this table required a lot of CPU time (on average a single computation using the stand-alone executable took 67.9 seconds to complete). The starting altitude was set at -0.6 km **MOLA** and advanced with a step-size of 0.1 km to 320 km altitude to cover the entire range that the **MAV** would have to cover. Also, the latitude and longitude were varied within 10 degrees from the launch site with a step-size of 1 degree. A Matlab script was written to extract the relevant atmospheric data from the **Mars-GRAM** output files and write them into a .csv file, thus creating the required atmospheric data table. The atmospheric data in this table was then interpolated to provide an estimate of the atmospheric characteristics at every point along the ascent trajectory, which is required to compute the drag at each time step. Some of the earlier versions of **Mars-GRAM** are available for free (such as the **Mars-GRAM** 2005 version used in this thesis), however, the latests versions (such as the **Mars-GRAM** 2010 version used as a back-up in this thesis) require a licence agreement.

## 7.2. DEVELOPED SOFTWARE

This section of the software chapter describes the software that either had to be developed around existing software/libraries or had to be developed from scratch (the **TSI** propagator). Each piece of software is accompanied by the corresponding software architecture. Every next piece of software then indirectly incorporates the previous architecture through the use of the completed tool.

### 7.2.1. ATMOSPHERIC TABLE FUNCTION FIT

Using **Mars-GRAM** 2005, a table containing altitude, latitude and longitude dependent temperature and density data was produced. The altitude range was -0.6 to 320 km **MOLA** with a step-size of 0.01 km, the latitude and longitude ranges were centred around the launch site (21.0 °N and 74.5 °E) with a 10 degree range in each direction and a step-size of 1 degree. The rest of the input parameters were constant and can be seen in Appendix A. The temperature and density data produced is shown in Figures 7.3 and 7.4 respectively for 9 latitude and longitude combinations including the launch site itself.

Unfortunately discontinuous data tables cannot be used when integrating using **TSI**, which is why both these data tables had to be fitted with continuous functions. The temperature data could not be smoothly fit with one continuous function. Therefore, depending on the altitude range, a different approximation function is required. The condition to be met for a proper fit came from the differences in the temperature-altitude and density-altitude curves, where the maximum difference with respect to the launch site curve was taken. The requirement for the standard deviation of the polynomial curve fit was then to be (at least) one order

<sup>4</sup>More documentation on **SNOPT** can be found on [http://www.sbsi-sol-optimize.com/asp/sol\\_products\\_snopt\\_desc.htm](http://www.sbsi-sol-optimize.com/asp/sol_products_snopt_desc.htm) [Accessed 9 March 2016]

<sup>5</sup>NASA website: <http://see.msfc.nasa.gov/model-Marsgram> [Accessed 9 March 2016]

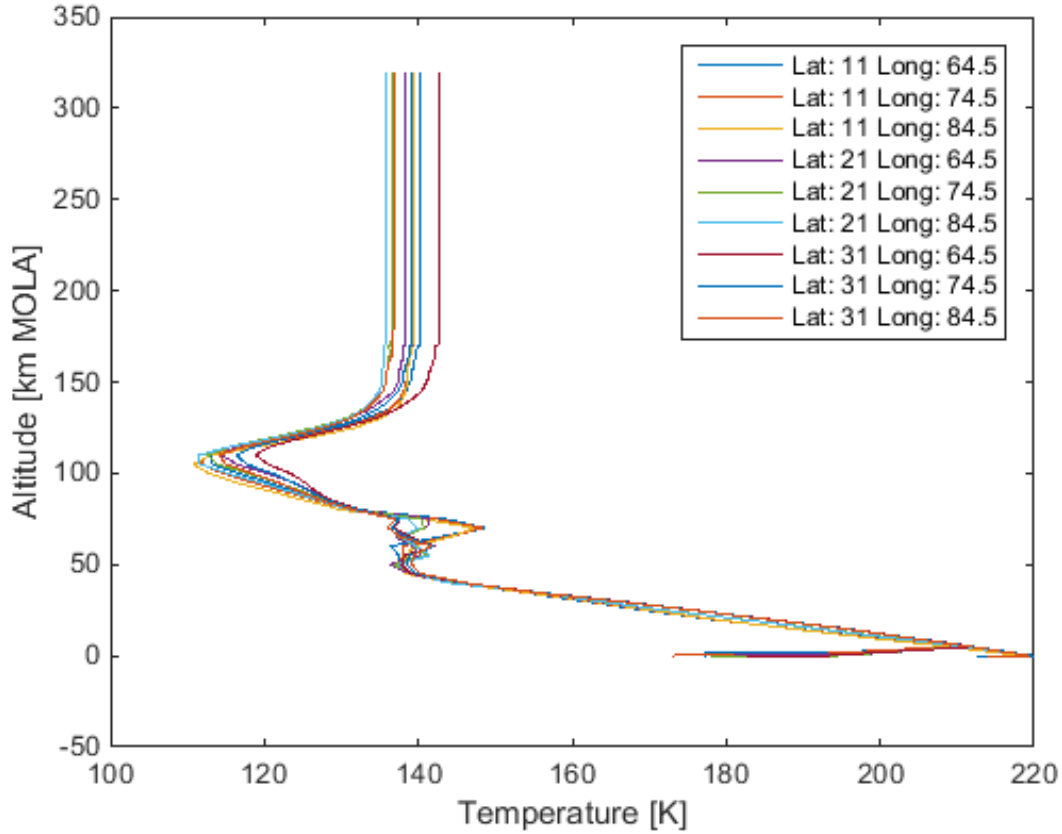


Figure 7.3: Temperature data generated with Mars-GRAM 2005 showing 9 different latitude and longitude combinations

lower than this maximum difference and that the maximum difference between the fit and the launch site curve was lower than the maximum difference. The temperature-altitude curve was split into 5 sections as roughly visualised in Figure 7.5. The number of sections come from both the shape of the curves and the requirement for accuracy and maximum order of the polynomial, which is set at 8 because otherwise the polynomial would get too long. Also, the number of sections were to be kept at a minimum. More information on the fitting process and early results is provided in Appendix B.

Each section was fit with a polynomial function of the  $n^{th}$  order where the function is represented by Equation (7.1). The last section shows a constant temperature, thus the temperature of the launch site curve was chosen to represent this final section.

$$y = p_n x^n + p_{n-1} x^{n-1} + \dots + p_1 x + p_0 \quad (7.1)$$

A lower order is preferred, because then the fitted function will be simpler to evaluate and contain fewer terms. However the order has to be high enough to meet the accuracy requirements. Table 7.1 shows the orders that were required and the deviations to the launch site temperature-altitude curve. The actual corresponding parameters are provided in Table 7.2. It should be noted that the first few temperature data values were so different from the rest of the curve that it was assumed that this is a lack of the Mars-GRAM program and were thus treated as outliers.

The complete polynomial fit for the launch site curve for the temperature is shown in Figure 7.6.

The density fit was slightly more difficult because the curves are all very similar and thus result in a higher accuracy requirement for the fit. At first glance it looks like a natural logarithmic function, unfortunately an ordinary exponential did not fit the curve. This is why a more extensive exponential fit was required. The natural logarithm of the data has been plotted in Figure 7.7.

With the data represented in the logarithmic domain, again a polynomial function can be fit. The total fit would then satisfy Equation (7.2).

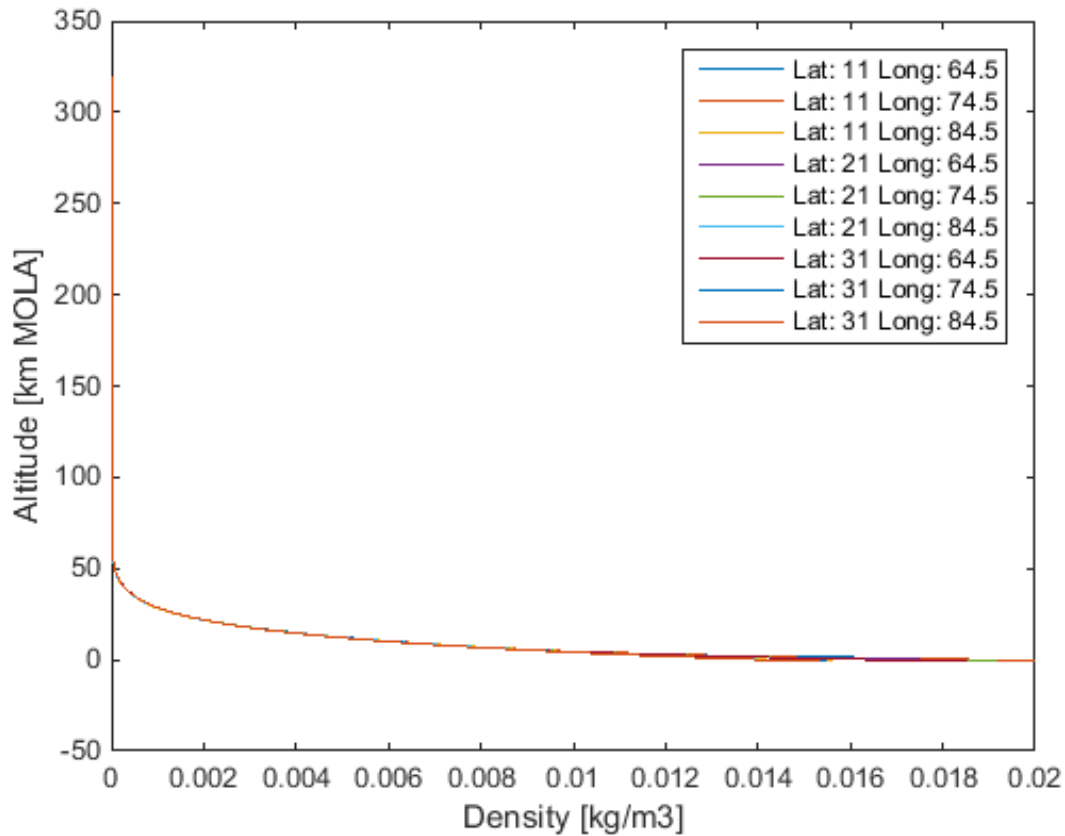


Figure 7.4: Density data generated with Mars-GRAM 2005 showing 9 different latitude and longitude combinations

Table 7.1: Temperature curve fit data all with respect to the launch site curve (Latitude and longitude of the launch site)

Section	Altitude range [km MOLA]	Order	Maximum poly-nomial standard deviation [K]	Maximum poly-nomial difference [K]	Maximum data curves difference [K]
1	-0.6 to 5.04	1	0.0312	25.8	0.177
2	5.04 to 35.53	2	0.287	3.90	0.7056
3	35.53 to 75.07	6	0.624	8.00	1.69
4	75.07 to 170.05	8	0.523	6.60	2.45

Table 7.2: Temperature curve fit parameters (rounded to 3 decimal points)

Section	p <sub>8</sub>	p <sub>7</sub>	p <sub>6</sub>	p <sub>5</sub>	p <sub>4</sub>	p <sub>3</sub>	p <sub>2</sub>	p <sub>1</sub>	p <sub>0</sub>
1								3.415	194.165
2							0.006	-2.130	222.052
3			-5.388 ·10 <sup>-7</sup>	1.785 ·10 <sup>-4</sup>	-0.0243	1.733	-68.294	1.407 ·10 <sup>3</sup>	-1.167 ·10 <sup>4</sup>
4	4.1942 ·10 <sup>-12</sup>	-4.328 ·10 <sup>-9</sup>	1.931 ·10 <sup>-6</sup>	-4.862 ·10 <sup>-4</sup>	0.076	-7.405	447.378	-1.523 ·10 <sup>4</sup>	2.236 ·10 <sup>5</sup>

$$y = \exp(p_n x^n + p_{n-1} x^{n-1} + \dots + p_1 x + p_0) \quad (7.2)$$

The same polynomial requirements as for the temperature curve were enforced for the density curve as

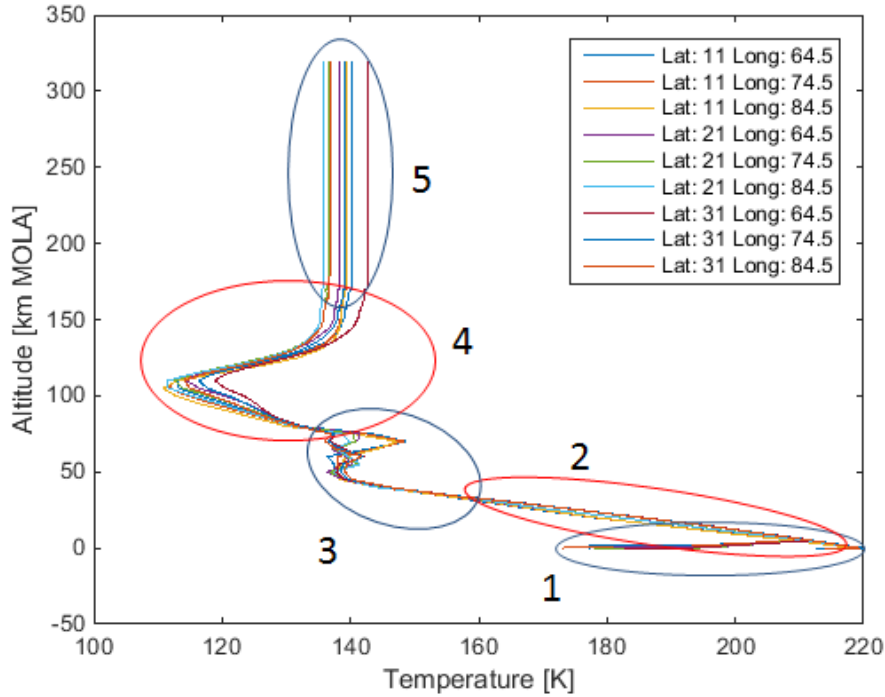


Figure 7.5: Different temperature curve sections

well. However, because the polynomial is used in an exponential, some extra requirements are needed to assure the accuracy of the fit. One requirement is that the maximum difference between the final exponential fit and the normal launch site density curve is smaller than the maximum difference between all the data curves. Also, in this case the standard deviation of the difference between the exponential fit and the normal launch site curve had to be within the range of standard deviations of the difference between the different data curves. This meant that even though an 8<sup>th</sup> order polynomial fit could be achieved for the natural logarithmic data with the required accuracy, when converted to the exponential fit, the last two requirements were not met. Before it was mentioned that an order higher than 8 was not desirable. However, in this case, a single exponential fit could be achieved using a 10<sup>th</sup> order polynomial. This fit meant that the density curve did not have to be split up at all, which makes the integration slightly easier. Therefore, it was decided that a 10<sup>th</sup> order polynomial was acceptable in this case. The results of the fit is presented in Tables 7.3 and 7.4 and the polynomial and exponential fit curves are shown in Figures 7.8 and 7.9 respectively.

Table 7.3: Density curve fit data (10<sup>th</sup> order polynomial) with respect to the launch site curve (Latitude and longitude of the launch site)

Maximum polynomial standard deviation [kg/m <sup>3</sup> ]	0.0501
Maximum polynomial difference [kg/m <sup>3</sup> ]	0.160
Maximum natural logarithmic data curves difference [kg/m <sup>3</sup> ]	0.460
Maximum exponential difference with launch site curve [kg/m <sup>3</sup> ]	2.826·10 <sup>-3</sup>
Maximum data curves difference [kg/m <sup>3</sup> ]	3.910·10 <sup>-3</sup>
Standard deviation exponential fit difference [kg/m <sup>3</sup> ]	1.167·10 <sup>-4</sup>
Maximum standard deviation data curves difference [kg/m <sup>3</sup> ]	2.106·10 <sup>-4</sup>

### 7.2.2.2. DRAG COEFFICIENT GRAPH FUNCTION FIT

Similar to the temperature and density curves, the relation between Mach number and drag coefficient, as depicted in Figure 7.10, had to be modelled as a continuous function as well. Again, it could not be fitted using one continuous function, but instead had to be modelled by different functions.

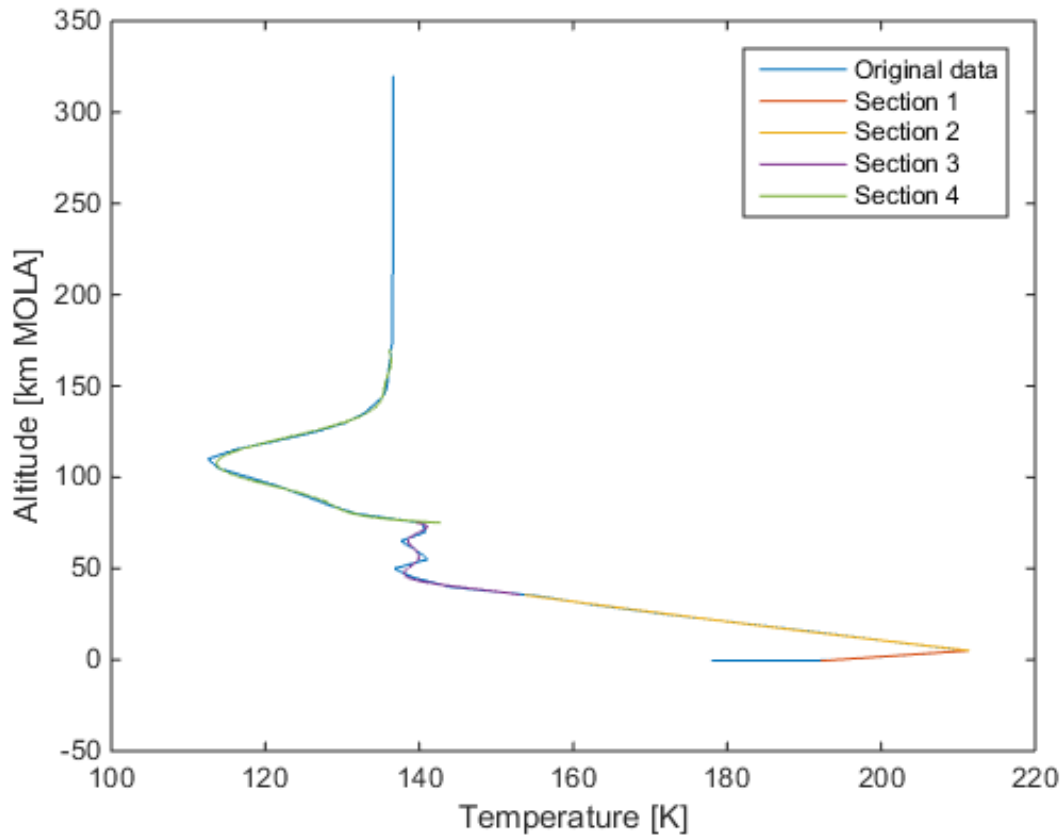


Figure 7.6: All section fits for the launch site temperature data curve

Table 7.4: Density curve fit parameters (rounded to 3 decimal points)

<b>P<sub>10</sub></b>	<b>P<sub>9</sub></b>	<b>P<sub>8</sub></b>	<b>P<sub>7</sub></b>	<b>P<sub>6</sub></b>	<b>P<sub>5</sub></b>	<b>P<sub>4</sub></b>	<b>P<sub>3</sub></b>	<b>P<sub>2</sub></b>	<b>P<sub>1</sub></b>	<b>P<sub>0</sub></b>
2.287 $\cdot 10^{-21}$	-3.724 $\cdot 10^{-18}$	2.559 $\cdot 10^{-15}$	-9.620 $\cdot 10^{-13}$	2.146 $\cdot 10^{-10}$	-2.884 $\cdot 10^{-8}$	2.273 $\cdot 10^{-6}$	-9.604 $\cdot 10^{-5}$	1.414 $\cdot 10^{-3}$	-0.0962	-4.172

Fortunately, this curve is already an approximation and thus consists of linear elements only. It can be split up into 6 different sections where the first and last section are constant. Using a similar polynomial fit as before, but now for 1 order only, a linear fit could be made for each of the remaining 4 sections. The corresponding parameters are shown in Table 7.5 and the curve fit is shown in Figure 7.11.

Table 7.5: Drag coefficient curve fit parameters (rounded to 3 decimal points)

<b>Section</b>	<b>Mach range</b>	<b>P<sub>1</sub></b>	<b>P<sub>0</sub></b>
2	0.5 to 1	0.400	$-2.483 \cdot 10^{-16}$
3	1 to 1.3	0.567	-0.167
4	1.3 to 2.5	-0.142	0.754
5	2.5 to 4	-0.0667	0.567

### 7.2.3. RK4 AND RKF PROPAGATOR

The **RK4** and **RKF** (or traditional) propagator architecture is described in Figure 7.12. It starts with the current state, which is then passed on to the state derivative function. The state derivative function is used by the **RK4** and **RKF** integrators to determine the next state by calling the function a number of times depending on the



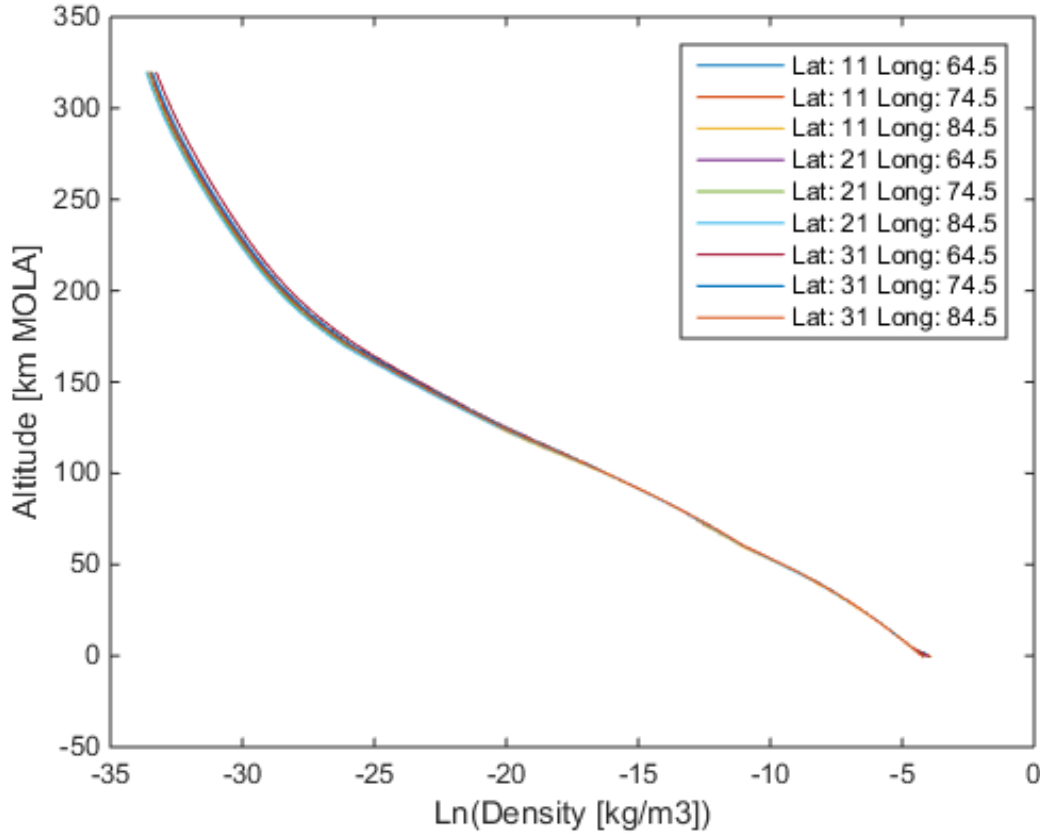


Figure 7.7: Natural logarithmic plot of the density data

used method. Both [RK4](#) and [RK45](#) (and higher order [RKF](#) integrators) are already available through the [Tudat](#) libraries. [RK4](#) can be called by including the `rungeKutta4Integrator.h` header file, and [RK45](#) can be called by including the `rungeKuttaVariableStepSizeIntegrator.h` header file. This integration process is repeated until the final condition is met. Within the state derivative function all the state derivatives are updated and stored. The current position is used to update the gravitational acceleration on the [MAV](#), the current mass is used to determine the accelerations caused by the thrust and finally the complete state is required to determine the accelerations caused by the drag. Both the drag and thrust accelerations have to be transformed to the inertial frame using the updated angles from the current state. The function also computes the current mass flow rate, however since the thrust is constant, this does not change over time. In the state derivative function, all the transformations are governed by pre-developed functions within the [Tudat](#) library, which includes the state transformations and the frame transformation from the body frame to the inertial frame. The transformation from the propulsion frame to the body frame is however not included in [Tudat](#) and had to be written.

#### 7.2.4. TSI PROPAGATOR

The [TSI](#) propagator has a significantly different architecture compared to the traditional propagator as can be seen in [Figure 7.13](#). [TSI](#) requires an initial order and step-size to start the integration process. In this thesis it has been decided to keep the order the same throughout the entire integration. The step-size will change during the integration depending on the Taylor series evaluations. The initial state is set as the current state and is fed into the [TSI](#) block. Within this block, first the auxiliary equations and functions are called, which were set-up for this particular problem. They are evaluated using the current state. These auxiliary equations and functions already include all the reference frame and coordinate transformations, as well as approximate atmospheric parameter functions. This is required to set-up the recurrence relations, which is where [TSI](#) differs from the traditional propagator. Once the auxiliary equations and functions have been computed they are used to compute the Taylor coefficients through the recurrence relations set-up for the thesis problem. These coefficients are then stored for later use and are also passed to the block creating the Taylor series

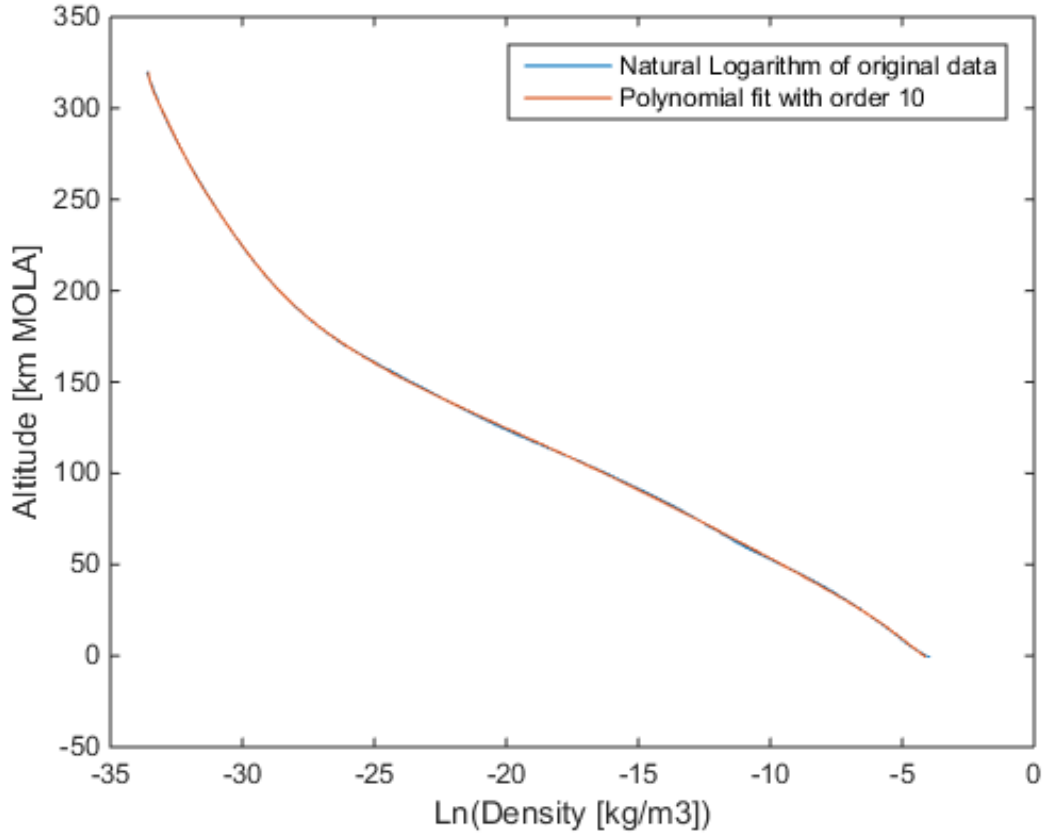


Figure 7.8: Polynomial fit for the launch site density data curve

expansion for every state variable thus creating the updated state. The last two coefficients are then used to determine the next step-size. This continues until the final integration condition has been met.

#### 7.2.5. OPTIMISER

The optimisation software is a combination of the [SNOPT](#) local optimisation tool and [PaGMO's MBH](#). Even though both these tools were already available and did not have to be developed, it is still important to understand how the rest of the software interacts with the optimiser. This is why Figure 7.14 shows the architecture of the [MBH](#) optimiser. It starts with the initial generation of the optimisation parameters, after which the 'Number of not improved iterations' is set to zero. This is then fed into the local optimiser, where the trajectory is integrated using the previously described tools. Once a local optimised trajectory is found, it is stored if it is better than the previous local optimised trajectory and the counter is set to zero again. If the newly found trajectory is not better than the current best the 'Number of not improved iterations' is increased by one. Once the maximum number of not improved iterations is met, the current best optimal trajectory (which is the optimum for the current "funnel") is stored and the process is repeated till the final global optimisation condition is met. At this point the global optimum is the best optimal trajectory from all the funnels computed at that time, which is then returned as the program solution.

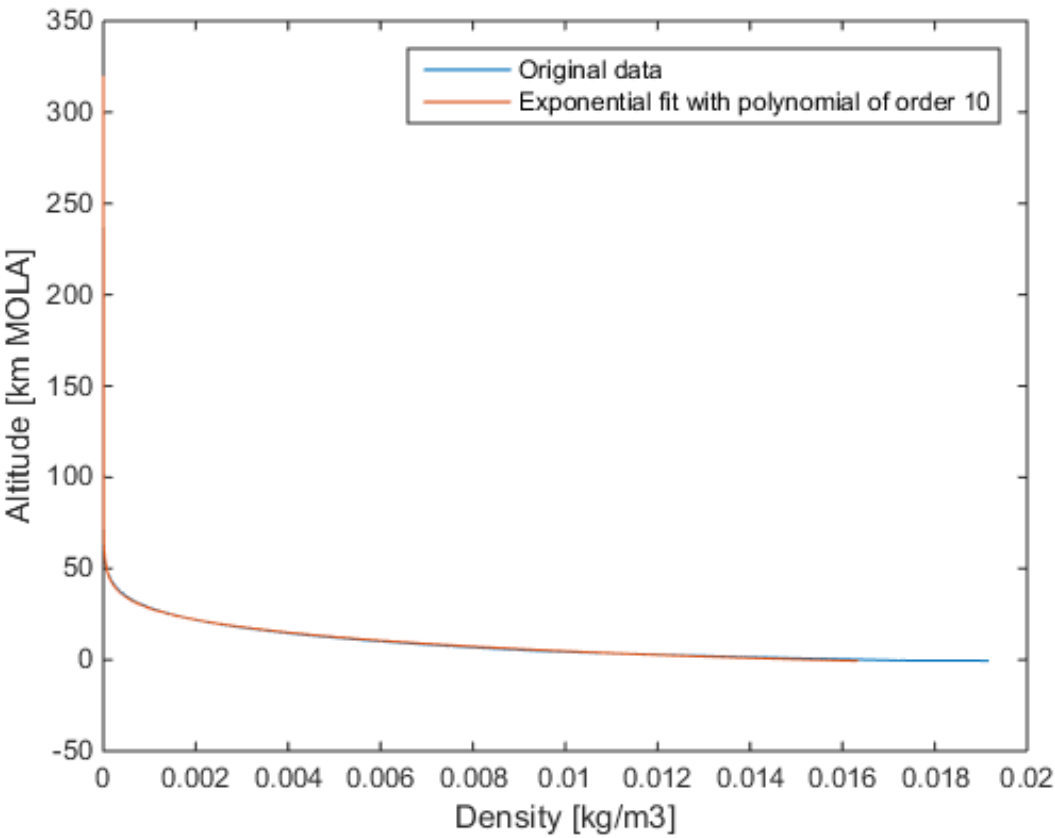


Figure 7.9: Exponential fit for the launch site density data curve

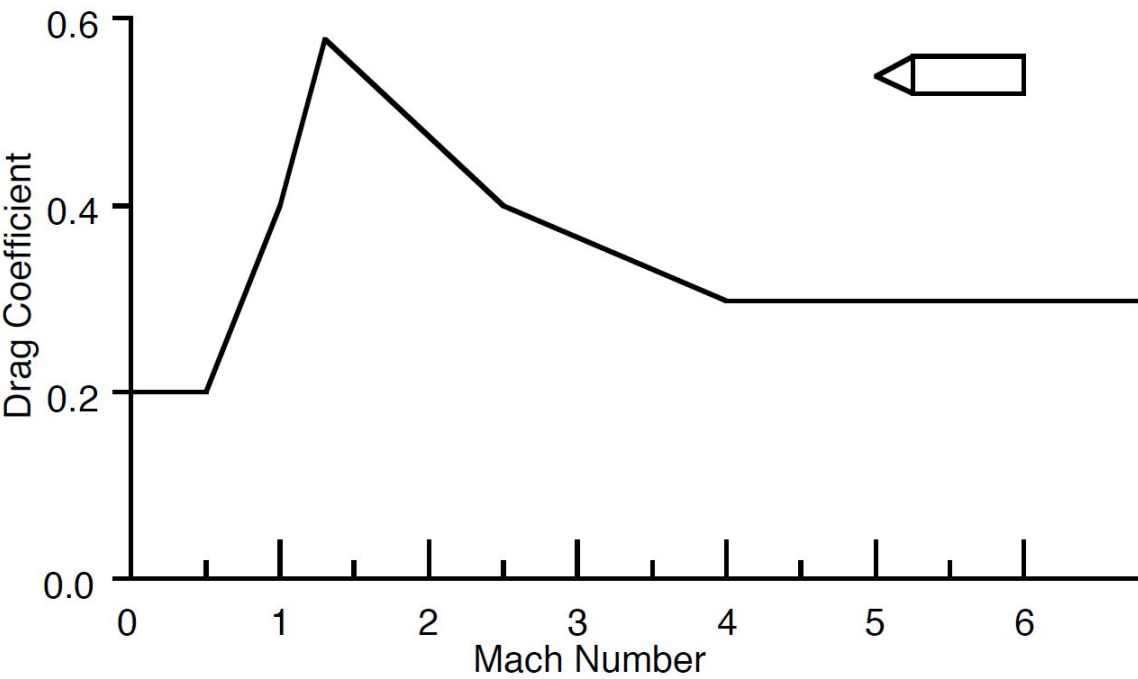


Figure 7.10: Drag coefficient as a function of Mach number [Whitehead \(2004\)](#)

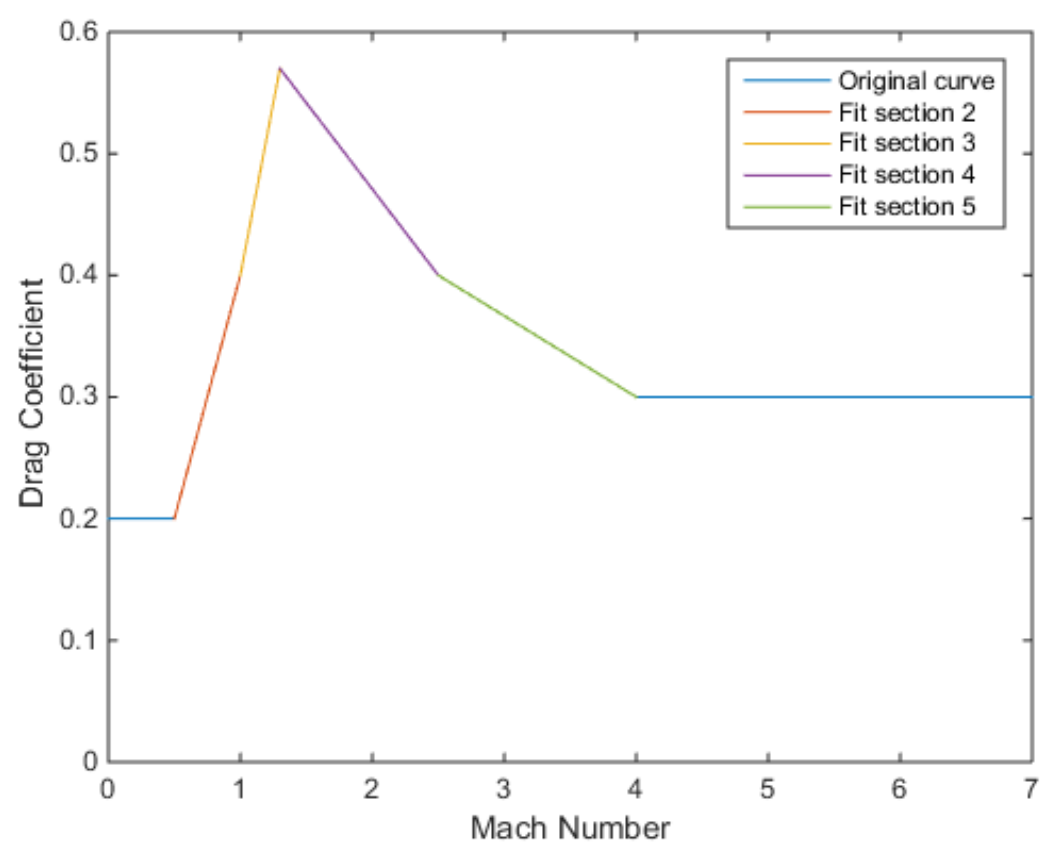


Figure 7.11: All section fits for the drag coefficient - Mach curve

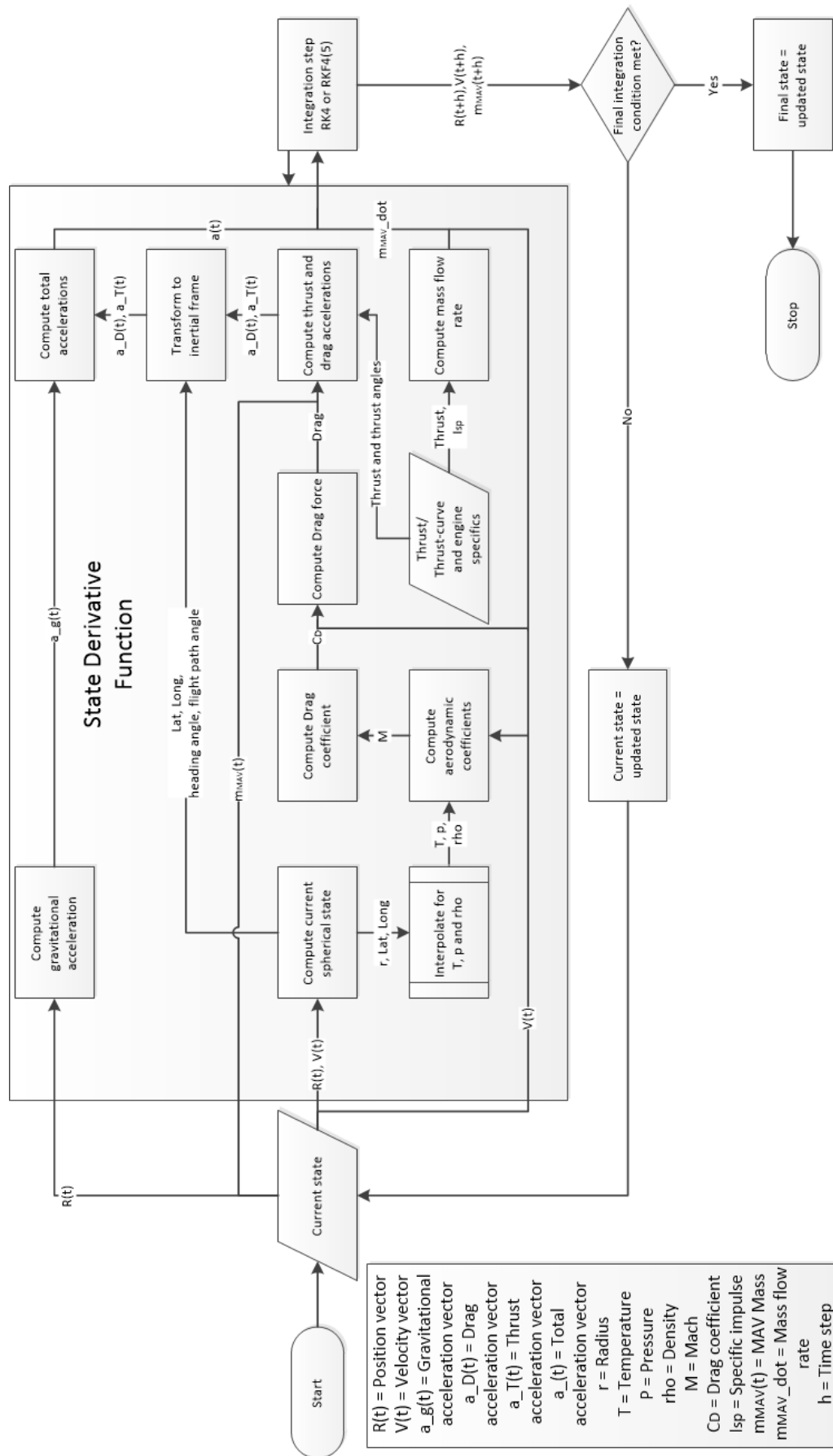


Figure 7.12: RK4 and RKF interface architecture

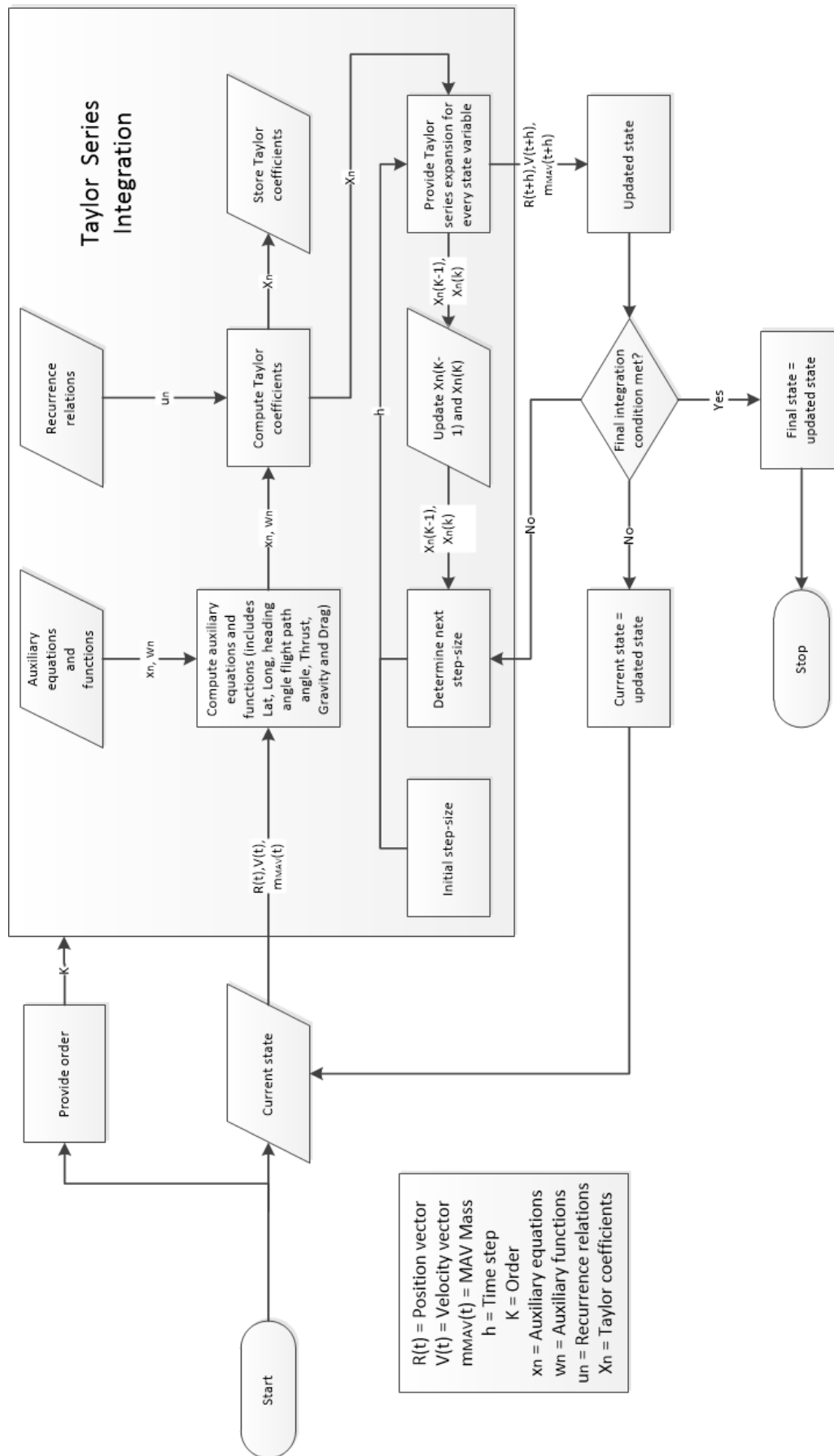


Figure 7.13: TSI architecture

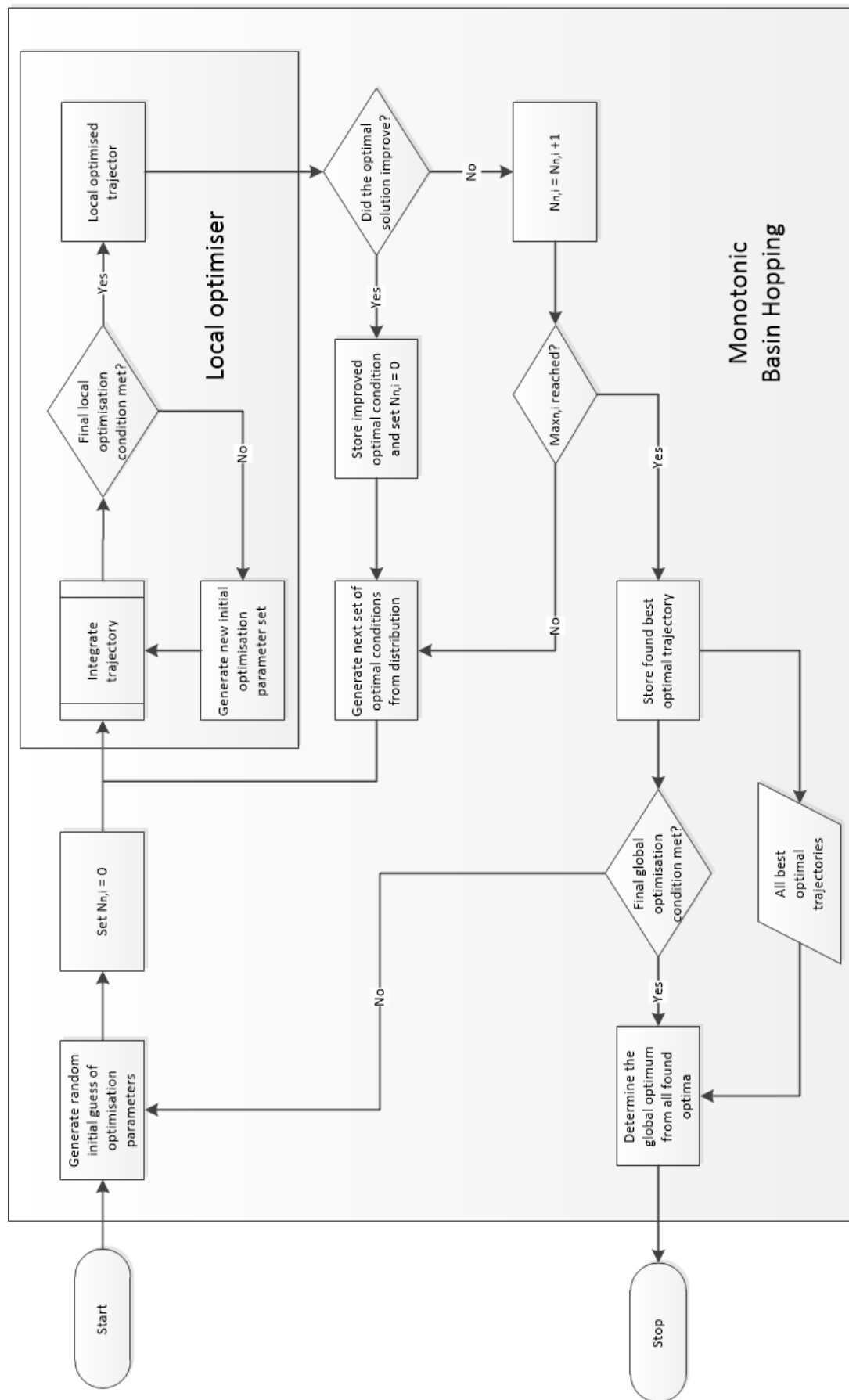


Figure 7.14: Optimiser interface architecture

# 8

## VERIFICATION AND VALIDATION

Verification is the process of determining whether a program meets the requirements or not. Is it working the way it is suppose to? As soon as it works and produces output (verified), these outputs can be compared to other data from which it is known that it is correct. This is called validation. If a program is verified and validated, the outputs should be correct. Fortunately, all the existing software has already been validated, which means that they only still have to be verified to make sure everything is working properly on the simulation computer. Each of the software packages comes with tests which can be used to do this. If all the tests are passed it means that the software is verified for the computer and ready to use. Since [Tudat](#) shipped with Eigen and Boost, the [Tudat](#) test files also test these libraries. All the test were passed, which means that the [Tudat](#), Eigen and Boost libraries are working properly. However, because the integrators are an intricate part of this thesis, it was decided to perform a separate verification for the Runge-Kutta integrators. This verification is described in Section 8.2. Similarly, [PaGMO](#) was verified using its test files.

**SNOPT verification still has to be done and added!! As soon as I can get it to work....**

Mars-GRAM also came with its own verification test, where three delivered output files had to be replicated. These verification tests were also successful.

### 8.1. INTERPOLATION

### 8.2. RK4 AND RKF INTEGRATORS

The tutorial page of the [Tudat](#) website ([Dirkx et al., 2016](#)) offers two integration tutorials: one involving [RK4](#) and another involving variable step-size Runge-Kutta methods including [RKF45](#). The objective of the tutorial is to get familiar with the different integration methods available in [Tudat](#). At the same time, a small data table has to be reproduced, which also serves as a verification test. For each of the integrators the same problem was addressed: the computation of the velocity of a falling body after a certain amount of time assuming no drag. The results that had to be reproduced are presented in Table 8.1.

Table 8.1: Verification data for the standard integrators

End time [s]	1.0	5.0	15.0	25.0
Velocity [m/s]	-9.81	-49.05	-147.15	-245.25

The first script was written using the instructions from the tutorial and is called `numericalintegrators.cpp`. This script uses the `rungeKutta4Integrator.h` header file and the `RungeKutta4IntegratorXd` function from this header file. This function requires three inputs: the state derivative function (problem specific), an initial time and the initial state. Using the `.integrateTo` extension the end state at a certain end time can be integrated. This requires the end time and the step-size. For [RK4](#) the step-size is constant. This resulted in the same values as presented in Table 8.1.

The second script was used to test the variable step-size integrators (including [RKF45](#)). This script is called `rungekuttavariable.cpp` and uses the `rungeKuttaCoefficients.h` and `rungeKuttaVariableStepSizeIntegrator.h`



header files. In this case the `RungeKuttaVariableStepSizeIntegratorXd` function was used which requires the Runge-Kutta coefficients (from the respective header file), the state derivative function, the initial time, initial state, zero minimum step-size, infinite maximum step-size, relative tolerance and the absolute tolerance as inputs. In this case the integration can be done in individual steps using `.performIntegrationStep` with the current step-size as the only input. The current step-size is computed in the integration method itself, but in this case it is checked to make sure that the step-size does not take the function beyond the specified end time. The integration steps are then repeated until the end time is met. Running this script resulted in the same results as presented in Table 8.1 as well.

These results, combined with the fact that the test files for these two methods produced no errors is proof that they are working accordingly. Thus it can be said that the standard integration methods used in this thesis are verified and ready for use in the optimisation tool. However, during the development of the trajectory propagation tools, the entire tool (including the integrators) will be verified again to determine the performance of the integrators.

### **8.3. TAYLOR SERIES INTEGRATION**

### **8.4. COMPLETE TRAJECTORY PROPAGATION**

### **8.5. OPTIMISER**

### **8.6. COMPLETE OPTIMISATION TOOL**

# 9

## RESULTS

# 10

ANALYSIS

# 11

## CONCLUSIONS AND RECOMMENDATIONS



## MARS-GRAM 2005 INPUT FILE

```
1 $INPUT
2   LSTFL   = 'LIST.txt'
3   OUTFL   = 'OUTPUT.txt'
4   TRAJFL  = 'TRAJDATA.txt'
5   profile = 'null'
6   WaveFile = 'null'
7   DATADIR = '/home/stachap/MarsGram/binFiles_TUdelft/'
8   GCMDIR  = '/home/stachap/MarsGram/binFiles_TUdelft/'
9   IERT     = 0
10  IUTC     = 1
11  MONTH    = 2
12  MDAY     = 28
13  MYEAR    = 2025
14  NPOS     = 32061
15  IHR      = 12
16  IMIN     = 0
17  SEC      = 0.0
18  LonEW    = 1
19  Dusttau  = 0
20  Dustmin  = 0.3
21  Dustmax  = 1.0
22  Dustnu   = 0.003
23  Dustdiam = 5.0
24  Dustdens = 3000.
25  ALSO     = 0.0
26  ALSDUR   = 48.
27  INTENS   = 0.0
28  RADMAX   = 0.0
29  DUSTLAT  = 0.0
30  DUSTLON  = 0.0
31  MapYear  = 0
32  F107     = 68.0
33  STDL     = 0.0
34  NR1      = 1234
35  NVARX    = 1
36  NVARX    = 0
37  LOGSCALE = 0
38  FLAT     = 21
39  FLON     = 74.5
40  FHGT     = -0.6
41  MOLAhgts = 1
42  hgtasfcm = 0.
43  zoffset  = 0.
44  ibougher = 0
45  DELHGT   = 0.01
46  DELLAT   = 0.0
47  DELLON   = 0.0
48  DELTIME  = 0.0
49  ΔTEX     = 0.0
```

```

50  profnear = 0.0
51  proffar = 0.0
52  rpscale = 1.0
53  rwscale = 1.0
54  wlscale = 1.0
55  wmscale = 0.0
56  blwinfac = 0.0
57  NMONTE = 1
58  iup = 13
59  WaveA0 = 1.0
60  WaveDate = 0.0
61  WaveA1 = 0.0
62  Wavephi1 = 0.0
63  phildot = 0.0
64  WaveA2 = 0.0
65  Wavephi2 = 0.0
66  phi2dot = 0.0
67  WaveA3 = 0.0
68  Wavephi3 = 0.0
69  phi3dot = 0.0
70  iuwave = 0
71  Wscale = 20.
72  corlmin = 0.0
73  ipclat = 1
74  requa = 3396.19
75  rpole = 3376.20
76  idaydata = 1
77  $END
78
79  Explanation of variables:
80  LSTFL = List file name (CON for console listing)
81  OUTFL = Output file name
82  TRAJFL = (Optional) Trajectory input file. File contains time (sec)
83           relative to start time, height (km), latitude (deg),
84           longitude (deg W if LonEW=0, deg E if LonEW=1, see below)
85  profile = (Optional) auxiliary profile input file name
86  WaveFile = (Optional) file for time-dependent wave coefficient data.
87            See file description under parameter iuwave, below.
88  DATADIR = Directory for COSPAR data and topographic height data
89  GCMDIR = Directory for GCM binary data files
90  IERT = 1 for time input as Earth-Receive time (ERT) or 0 Mars-event
91        time (MET)
92  IUTC = 1 for time input as Coordinated Universal Time (UTC), or 0
93        for Terrestrial (Dynamical) Time (TT)
94  MONTH = (Integer) month of year
95  MDAY = (Integer) day of month
96  MYEAR = (Integer) year (4-digit; 1970-2069 can be 2-digit)
97  NPOS = max # positions to evaluate (0 = read data from trajectory
98        input file)
99  IHR = Hour of day (ERT or MET, controlled by IERT and UTC or TT,
100       controlled by IUTC)
101  IMIN = minute of hour (meaning controlled by IERT and IUTC)
102  SEC = seconds of minute (meaning controlled by IERT and IUTC).
103       IHR:IMIN:SEC is time for initial position to be evaluated
104  LonEW = 0 for input and output West longitudes positive; 1 for East
105          longitudes positive
106  Dusttau = Optical depth of background dust level (no time-developing
107            dust storm, just uniformly mixed dust), 0.1 to 3.0, or use
108            0 for assumed seasonal variation of background dust
109  Dustmin = Minimum seasonal dust tau if input Dusttau=0 ( $\geq 0.1$ )
110  Dustmax = Maximum seasonal dust tau if input Dusttau=0 ( $\leq 1.0$ )
111  Dustnu = Parameter for vertical distribution of dust density (Haberle
112          et al., J. Geophys. Res., 104, 8957, 1999)
113  Dustdiam = Dust particle diameter (micrometers, assumed monodisperse)
114  Dustdens = Dust particle density (kg/m3)
115  ALS0 = starting Ls value (degrees) for dust storm (0 = none)
116  ALSDUR = duration (in Ls degrees) for dust storm (default = 48)
117  INTENS = dust storm intensity (0.0 - 3.0)
118  RADMAX = max. radius (km) of dust storm (0 or >10000 = global)
119  DUSTLAT = Latitude (degrees) for center of dust storm
120  DUSTLON = Longitude (degrees) (West positive if LonEW=0, or East

```

```

121         positive if LonEW = 1) for center of dust storm
122 MapYear = 1 or 2 for TES mapping year 1 or 2 GCM input data, or 0 for
123           Mars-GRAM 2001 GCM input data sets
124 F107 = 10.7 cm solar flux (10**-22 W/cm**2 at 1 AU)
125 NR1 = starting random number (0 < NR1 < 30000)
126 NVARX = x-code for plotable output (1=hgt above MOLA areoid).
127         See file xycodes.txt
128 NVARY = y-code for 3-D plotable output (0 for 2-D plots)
129 LOGSCALE = 0=regular SI units, 1=log-base-10 scale, 2=percentage
130             deviations from COSPAR model, 3=SI units, with density
131             in kg/km**3 (suitable for high altitudes)
132 FLAT = initial latitude (N positive), degrees
133 FLON = initial longitude (West positive if LowEW = 0 or East
134         positive if LonEW = 1), degrees
135 FHGT = initial height (km); ≤-10 means evaluate at surface height;
136         > 3000 km means planeto-centric radius
137 MOLAhgts = 1 for input heights relative to MOLA areoid, otherwise
138             input heights are relative to reference ellipsoid
139 hgtasfcm = height above surface (0-4500 m); use if FHGT ≤ -10. km
140 zoffset = constant height offset (km) for MTGCM data or constant
141           part of Ls-dependent (Bougher) height offset (0.0 means
142           no constant offset). Positive offset increases density,
143           negative offset decreases density.
144 ibougher = 0 for no Ls-dependent (Bougher) height offset term; 1
145             means add Ls-dependent (Bougher) term, -A*Sin(Ls) (km),
146             to constant term (zoffset) [offset amplitude A = 2.5 for
147             MapYear=0 or 0.5 for MapYear > 0]; 2 means use global mean
148             height offset from data file hgtoffset.dat; 3 means use
149             daily average height offset at local position; 4 means
150             use height offset at current time and local position.
151             Value of zoffset is ignored if ibougher = 2, 3, or 4.
152 DELHGT = height increment (km) between steps
153 DELLAT = Latitude increment (deg) between steps (Northward positive)
154 DELLOn = Longitude increment (deg) between steps (Westward positive
155           if LonEW = 0, Eastward positive if LonEW = 1)
156 DELTIME = time increment (sec) between steps
157 ΔTEX = adjustment for exospheric temperature (K)
158 profnear = Lat-lon radius (degrees) within which weight for auxiliary
159            profile is 1.0 (Use profnear = 0.0 for no profile input)
160 proffar = Lat-lon radius (degrees) beyond which weight for auxiliary
161           profile is 0.0
162 rpscale = random density perturbation scale factor (0-2)
163 rwscale = random wind perturbation scale factor (≥0)
164 wlscale = scale factor for perturbation wavelengths (0.1-10)
165 wmscale = scale factor for mean winds
166 blwinfac = scale factor for boundary layer slope winds (0 = none)
167 NMONTE = number of Monte Carlo runs
168 iup = 0 for no LIST and graphics output, or unit number for output
169 WaveA0 = Mean term of longitude-dependent wave multiplier for density
170 WaveDate = Julian date for (primary) peak(s) of wave (0 for no traveling
171            component)
172 WaveA1 = Amplitude of wave-1 component of longitude-dependent wave
173           multiplier for density
174 Wavephi1 = Phase of wave-1 component of longitude-dependent wave
175            multiplier (longitude, with West positive if LonEW = 0,
176            East positive if LonEW = 1)
177 phildot = Rate of longitude movement (degrees per day) for wave-1
178            component (Westward positive if LonEW = 0, Eastward
179            positive if LonEW = 1)
180 WaveA2 = Amplitude of wave-2 component of longitude-dependent wave
181           multiplier for density
182 Wavephi2 = Phase of wave-2 component of longitude-dependent wave
183            multiplier (longitude, with West positive if LonEW = 0,
184            East positive if LonEW = 1)
185 phi2dot = Rate of longitude movement (degrees per day) for wave-2
186            component (Westward positive if LonEW = 0, Eastward
187            positive if LonEW = 1)
188 WaveA3 = Amplitude of wave-3 component of longitude-dependent wave
189           multiplier for density
190 Wavephi3 = Phase of wave-3 component of longitude-dependent wave
191            multiplier (longitude, with West positive if LonEW = 0,

```

```

192      East positive if LonEW = 1)
193  phi3dot = Rate of longitude movement (degrees per day) for wave-3
194            component (Westward positive if LonEW = 0, Eastward
195            positive if LonEW = 1)
196  iuwave  = Unit number for (Optional) time-dependent wave coefficient
197            data file "WaveFile" (or 0 for none).
198            WaveFile contains time (sec) relative to start time, and
199            wave model coefficients (WaveA0 thru Wavephi3) from the
200            given time to the next time in the data file.
201  Wscale  = Vertical scale (km) of longitude-dependent wave damping
202            at altitudes below 100 km ( $10 \leq Wscale \leq 10,000$  km)
203  corlmin = minimum relative step size for perturbation updates
204            (0.0-1.0); 0.0 means always update perturbations, x.x
205            means only update perturbations when corlim > x.x
206  ipclat  = 1 for Planeto-centric latitude and height input,
207            0 for Planeto-graphic latitude and height input
208  requa   = Equatorial radius (km) for reference ellipsoid
209  rpole   = Polar radius (km) for reference ellipsoid
210  idaydata = 1 for daily max/min data output; 0 for none

```



# B

## ATMOSPHERIC DATA FITTING

In Section 7.2.1 the final results of the atmospheric data fits were presented. However, before those results could be obtained, a few iterations of trial-and-error fits were required. These intermediate trials are presented for both the temperature data, in Appendix B.1, as well as for the density data, in Appendix B.2. The fit requirements for the polynomial function were set such that the errors created by the fit were less than the uncertainty of the latitude and longitude dependent data. This way the desired accuracy could still be reached. This uncertainty is caused by the difference in atmospheric data curves for the different latitudes and longitudes. The atmospheric data curve for the latitude and longitude corresponding to the launch site (21.0 °N and 74.5 °E) was taken as the reference curve and called the launch site curve. The differences between this launch site curve and the 8 other curves were used to define the maximum data curves difference. The *polyfit.m* function within Matlab was used to fit a polynomial to the data. This function also directly provides a standard deviation of the fit for each data point (in combination with the *polyval.m* function). One of the requirements was for the maximum standard deviation of the polynomial fit to be one order less than the maximum difference of the data curves with respect to the launch site curve. The second requirements for a proper fit was for the absolute maximum difference between the polynomial fit and the launch site curve to be less than the absolute maximum difference between the data curves and that same launch site curve.

### B.1. TEMPERATURE

Initially, the temperature data curve was split into 6 different sections as portrayed in Figure B.1. The sections were selected on the basis of their individual shapes and the maximum order that was required, where the maximum order for temperature was set at 8. Fewer sections were however always preferred.

Unfortunately, the fourth quarter of section 3 caused this section to not meet the maximum standard deviation requirement because in that quarter the linear behaviour changes directions slightly and the differences between the different data curves become a lot smaller. Therefore section 3 was split into two different sections resulting in a total of 7 sections as shown in Figure B.2.

These sections all met the requirements and thus provided a proper fit to the data. This fit is shown in Figure B.3.

However, because fewer sections were preferred, an attempt was made to reduce the number of sections. Because of the inaccuracy in the Mars-GRAM model close to the planet surface, it was decided to delete the outliers near the surface (section 1) and stretch the outcome of the second polynomial fit to the surface instead. Also, it turned out that section 4 and 5 could be combined in such a way that the requirements were still met. This reduced the number of section from 7 to 5. The final fit was presented in Section 7.2.1 as well as the corresponding errors and polynomial coefficients.

### B.2. DENSITY

For the density curve, because the data represents a logarithmic curve, initially an exponential atmosphere was fit. However, this did not meet any of the requirements for a proper fit as can be seen in . This is why a polynomial fit was attempted for the density curve as well with the same requirement as the temperature fits. The first fit was attempted with two sections as presented in Figure B.4.

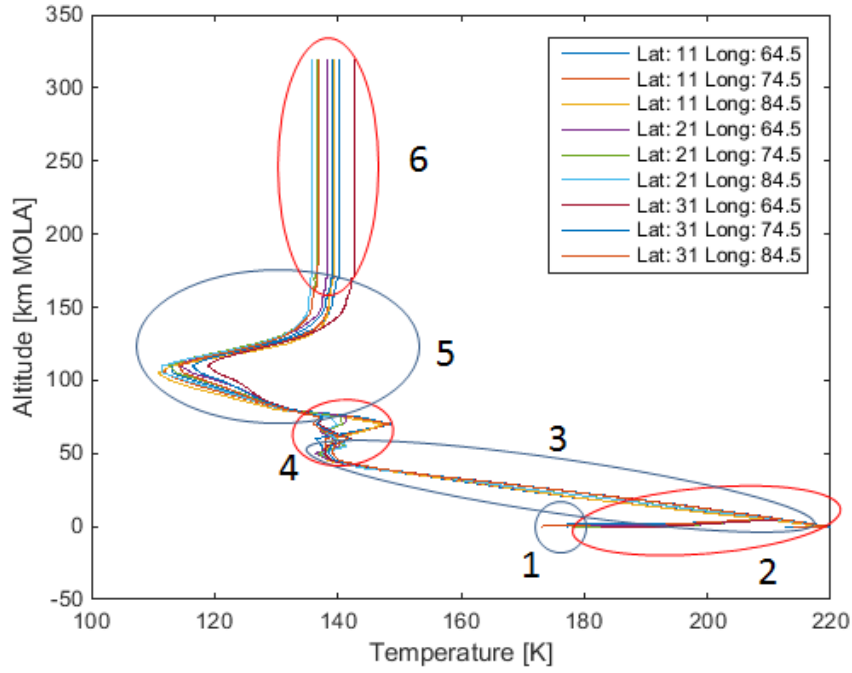


Figure B.1: Six different temperature curve sections

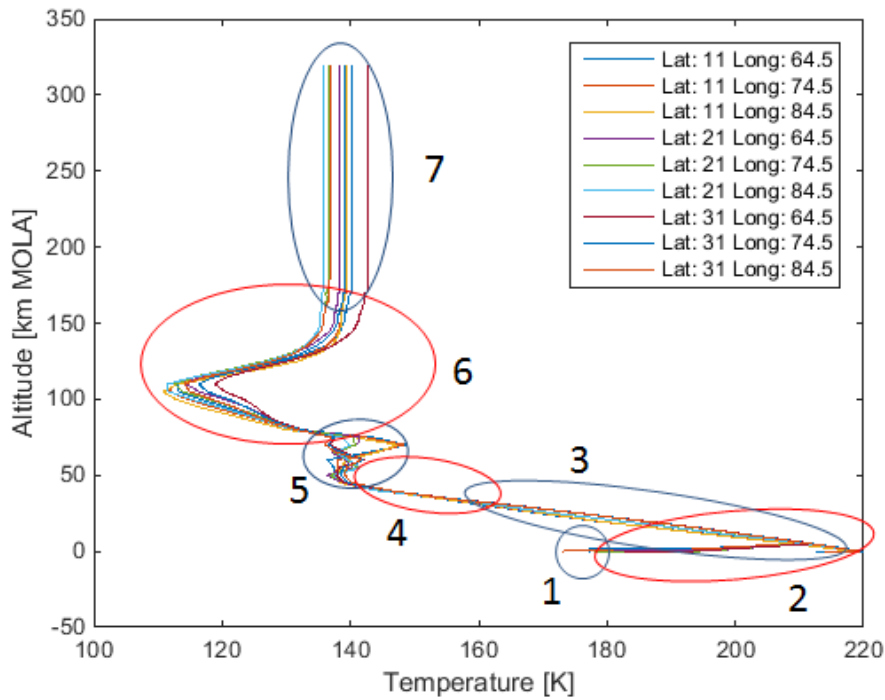


Figure B.2: Seven different temperature curve sections

However, the second section could not meet the requirements because of the initial part. This is why it was split into two sections as presented in Figure B.5.

This did meet the error requirements and resulted in the fit as shown in Figure B.6 with section 1 being

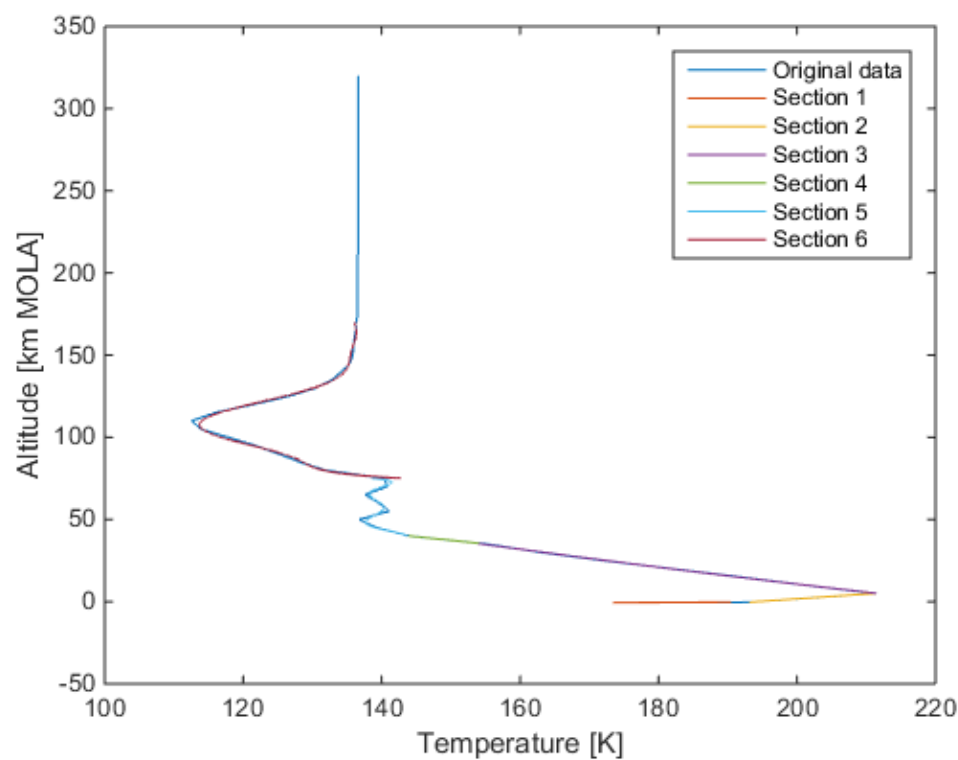


Figure B.3: All section fits for the launch site temperature data curve

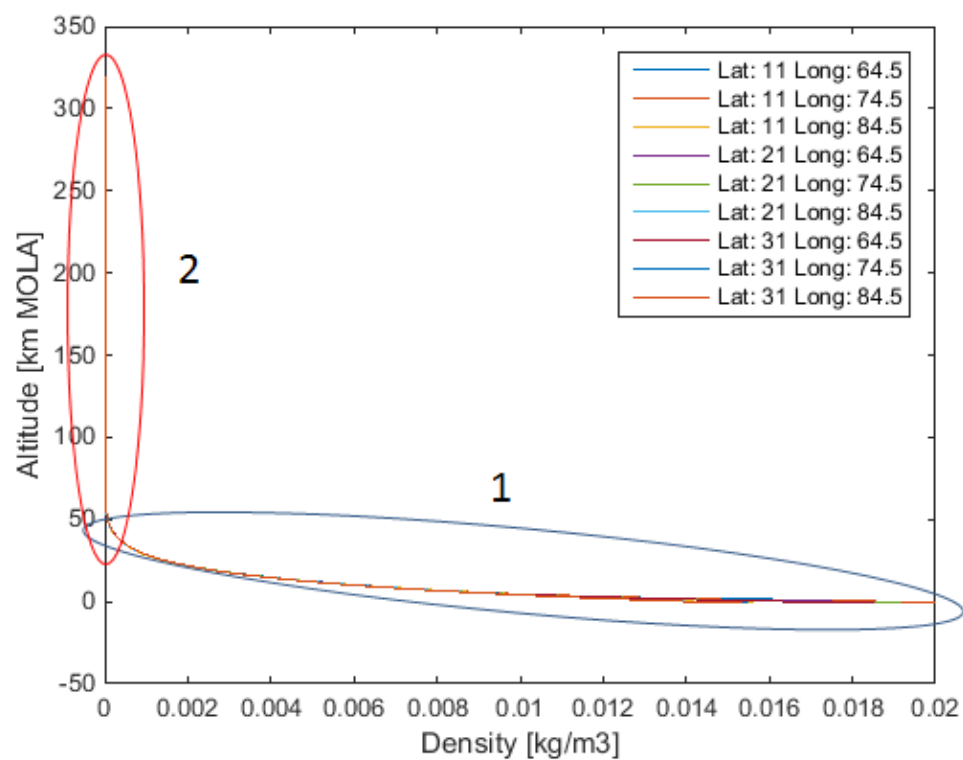


Figure B.4: Two different density curve sections

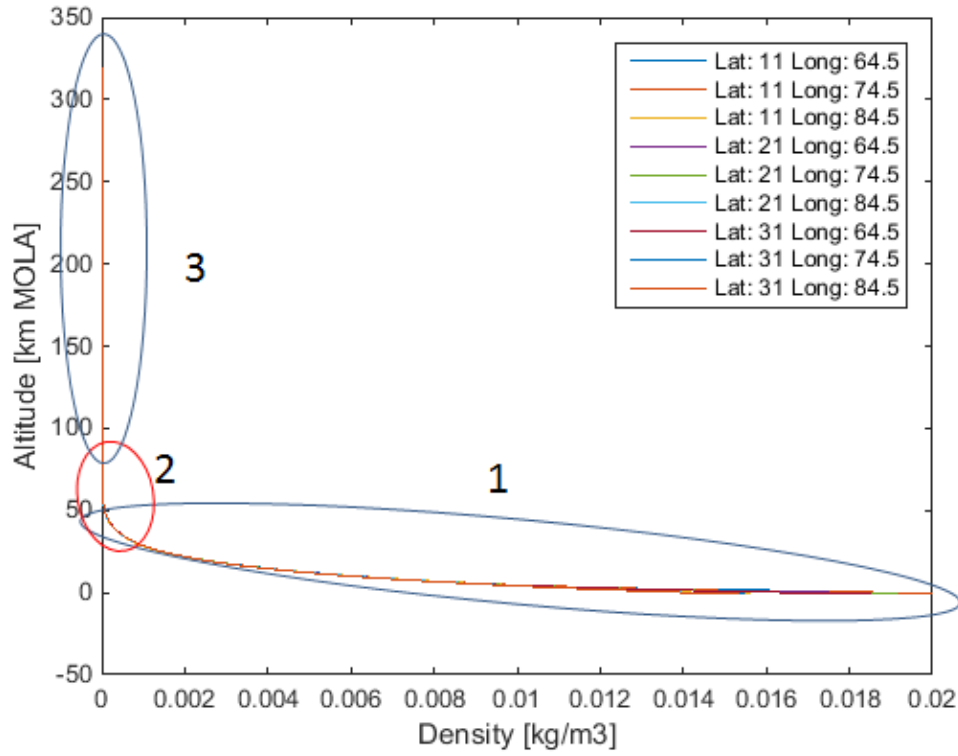


Figure B.5: Three different density curve sections

the lower part, section 2 the middle and section 3 the upper part.

However, in this case the fit for section three resulted in an oscillating behaviour around the actual data which caused the density values to drop below zero as shown in Figure B.7. Since this is unrealistic, an exponential atmospheric fit for only the third section was attempted (also shown in Figure B.7) however, this resulted in the same behaviour as the attempt for the entire curve. Therefore, it was decided to try a different exponential approach which eventually resulted in the fit described in Section 7.2.1.

Figure B.8 clearly shows that both the full exponential atmospheric fit and the polynomial fits were not a proper choice here. The figure shows the curved part of the curve.

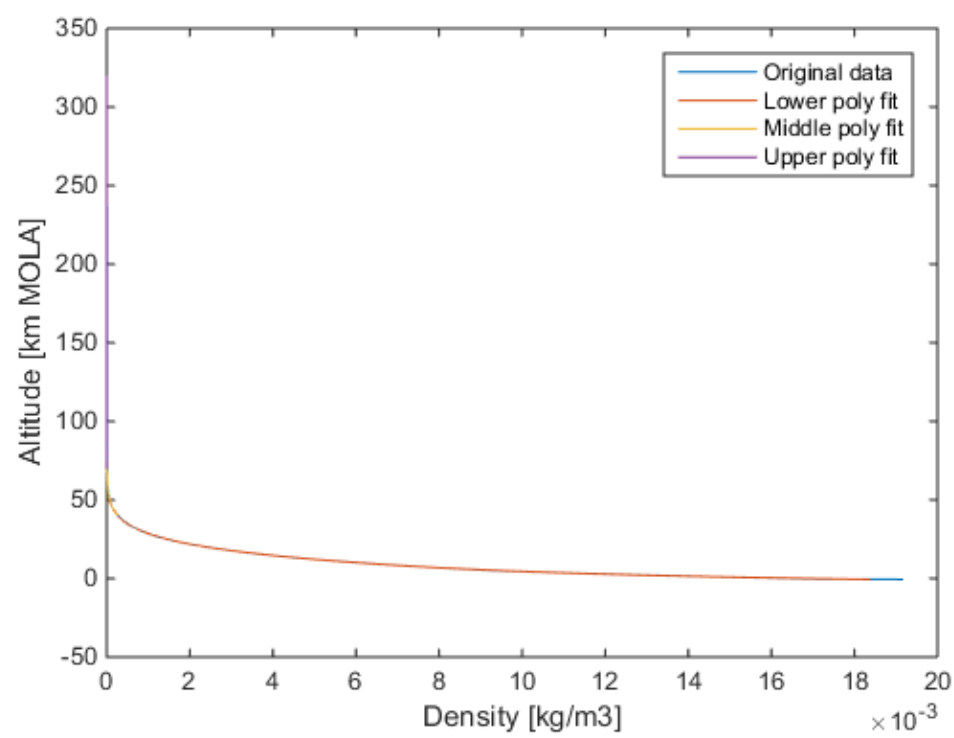


Figure B.6: All section fits for the launch site density data curve

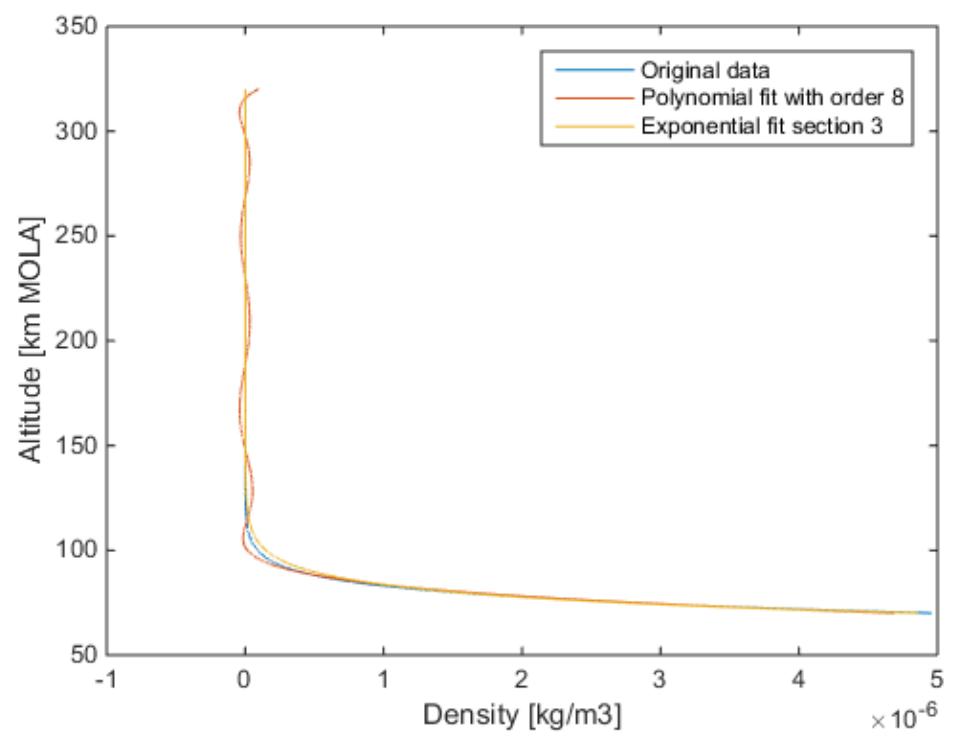


Figure B.7: Section 3 fit for the launch site density data curve

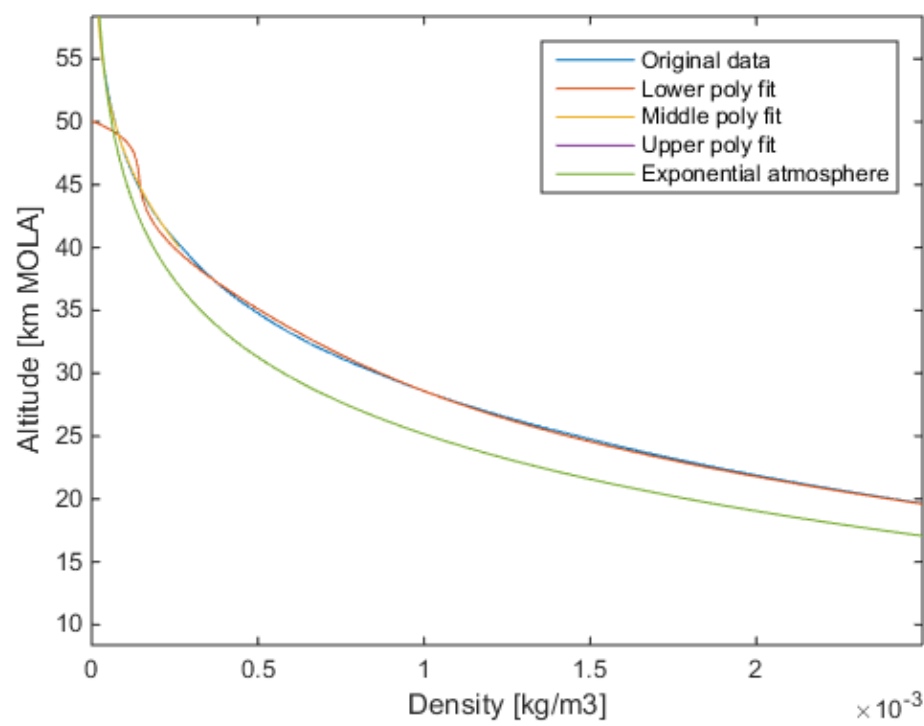


Figure B.8: Zoom in of the end of section 1 with the polynomial and exponential atmospheric fits

# BIBLIOGRAPHY

- J. R. Scott and M. C. Martini, *High speed solution of spacecraft trajectory problems using Taylor series integration*, in *AIAA/AAS Astrodynamics Specialist Conference and Exhibit, Honolulu, Hawaii* (2008).
- R. Noomen, *ae4-878.basics.v4-14*, Lecture slides, Delft University of Technology (2013), [Internal publication] Course: Mission Geometry and Orbit Design.
- D. Dirkx, K. Kumar, E. Doornbos, E. Mooij, and R. Noomen, *TUDAT*, (2016), [online database], URL: [tudat.tudelft.nl](http://tudat.tudelft.nl) [cited 8 March 2016] (Only available from the TU Delft network).
- A. Qing, *Differential Evolution: Fundamentals and Applications in Electrical Engineering* (John Wiley & Sons, Singapore, 2009).
- D. Izzo, *PyGMO and PyKEP: Open source tools for massively parallel optimization in astrodynamics (the case of interplanetary trajectory optimization)*, in *5th International Conference on Astrodynamics Tools and Techniques (ICATT)* (2012).
- P. E. Gill, W. Murray, and M. A. Saunders, *SNOPT: An SQP algorithm for large-scale constrained optimization*, in *SIAM journal on optimization*, Vol. 12 (2002) pp. 979–1006.
- P. E. Gill, W. Murray, and M. A. Saunders, *Users guide for SNOPT version 7 - Software for large-scale nonlinear programming*, (2008), [online database], URL: <http://web.stanford.edu/group/SOL/guides/> [cited 23 October 2015].
- H. L. Justh and C. G. Justus, *Utilizing Mars global reference atmospheric model (Mars-GRAM 2005) to evaluate entry probe mission sites*, Presentation (2008), [online database], URL: <https://smartech.gatech.edu/bitstream/handle/1853/26375/34-186-1-PB.pdf?sequence=1> [cited 10 December 2015].
- J. C. Whitehead, *Mars Ascent Propulsion Trades with Trajectory Analysis*, in *40th AIAA/ASME/SAE/ASEE Joint Propulsion Conference and Exhibit* (American Institute of Aeronautics and Astronautics, 2004).